# A Novel Magnetic Resonance Imaging Technique to Assess Tissue Viability Following Acute Myocardial Infarction: Simultaneous T1 and T2* Signal Intensity Monitoring Following Bolus Injected Contrast Agent.

By

John K. Mark

A thesis submitted for the degree of

Master of Science

Department of Physiology, University of Manitoba

THE UNIVERSITY OF MANITOBA

FACULTY OF GRADUATE STUDIES

*****

COPYRIGHT PERMISSION PAGE

# A Novel Magnetic Resonance Imaging Technique to Assess Tissue Viability Following Acute Myocardial Infarction: Simultaneous T1 and T2* Signal Intensity Monitoring Following Bolus Injected Contrast Agent

BY

John K. Mark

A Thesis/Practicum submitted to the Faculty of Graduate Studies of The University of Manitoba in partial fulfillment of the requirements of the degree of

Master of Science

*To the friends I have made at the National Research Council – Institute for Biodiagnostics. Thank you for all your support and patience.*

# Table of Contents

# Abstract

This study was designed to determine whether injured myocardium can be identified by simultaneously monitoring contrast-induced T1 and T2* signal intensity changes with an interleaved T1-T2* imaging sequence and to compare these results to techniques that calculate relaxation rate following contrast agent injection.

Eight pigs were subjected to *in situ* coronary artery occlusion for 2 hours, followed by 1-hour of reperfusion. The hearts were then excised and imaged *ex vivo*. Gadolinium-diethylene triamine pentaacetic acid (0.05 mmol/kg) was injected as a bolus and T1 and T2* signal intensities were monitored using alternating T1 and T2*-weighted imaging to obtain simultaneous T1 and T2* timecourses during the first pass. The T2* signal at maximum T1 signal intensity displayed a percentage recovery that was significantly different ($p < 0.05$) between normal (30.5 ± 2.4 % of baseline value), reperfused-infarcted (63 ± 7.2 %), and low-reflow infarcted myocardium (90 ± 2.8 %) respectively. This may reflect differences in membrane integrity between regions. On the other hand, R1 and R2* relaxation rates did not show any significant difference ($p > 0.05$) in the low-reflow infarcted myocardium relative to normal tissue. These results suggest that observing contrast-enhanced R1 and R2* rates early after contrast injection cannot fully differentiate viable from non-viable myocardium, but simultaneously monitoring both T1 and T2* signal intensity may help in the assessment of myocardial injury.

## Acknowledgments

I would like to take a moment to acknowledge all the support and patience I have received from the researchers, technicians, animal care, and support staff at the National Research Council, Institute for Biodiagnostics. In particular I would like to thank doctors Roxanne Deslauriers and Hong Tian for their abundant guidance over the last two years. I would also like to express my gratitude to Mrs. Lori Gregorash and Allan Turner for tolerating me in their surgery. Lastly, I want to thank Rick Mangat for being kind enough to let me share his office.

## Statement

The work reported in this thesis was undertaken at the National Research Council, Institute for Biodiagnostics in conjunction with the Department of Physiology at the University of Manitoba. Supervision of this work was provided by Dr. Roxanne Deslauriers and Dr. Ganghong Tian.

I declare that the content present within this thesis is original and that the materials contained herein have not been submitted either in part of in full for a degree at this or any other university.

John K. Mark

December 18, 2000

# List of Figures

# 1. Introduction

The assessment of myocardial viability is a major goal because it will allow the cardiologist to differentiate patients suffering reversible ventricular dysfunction from those with irreversible damage. The information can guide patient management decisions by distinguishing which individuals will gain the most benefit from the revascularization and transplantation options that are available (1-5). Hopefully, improved identification and resource allocation can lead to better patient care.

The techniques that are currently in use to evaluate myocardial viability include single photon emission computed tomography (SPECT), positron emission tomography (PET), and echocardiography. However, these diagnostic methods suffer from poor spatial resolution with pixel sizes in the range of 0.5-1 $cm^2$. In addition, SPECT and PET utilize radioactive tracer materials. These are limitations that make the development of a new measure of tissue viability very appealing (6-8).

We believe that with its superior spatial resolution, magnetic resonance imaging (MRI) can be used to gauge tissue damage more effectively. In previous studies, contrast-enhanced MRI has been used to distinguish irreversibly damaged tissues using either T1 or T2*-weighted imaging by probing cell membrane integrity (9, 10). These techniques rely on a homogenous distribution of contrast agent throughout the heart. However, flow affects the extracellular concentration of a contrast agent (11). Because perfusion within an infarct may not be homogenous, contrast agents may not be evenly distributed to all regions similarly leading to zones of hypoenhanced and hyperenhanced infarct (12).

One method that has been proposed to circumvent this limitation is to continually infuse an MR contrast agent until equilibrium levels are reached in the heart (13, 14).

While this method has shown promising results, it requires additional patient preparation time and administration of large amounts of contrast agent. Due to the nature of these agents, this approach would be unsuitable for patients with depressed renal function (15). Additionally, these techniques do not appear very good at identifying regions of reversibly damaged tissue or regions of damage that include pleomorphic populations of viable and non-viable cells (16).

## 1.1. Hypothesis

To improve the reliability of an MR diagnosis, we hypothesized that a combined T1 and T2*-weighted technique could be used. This is because T1-weighted imaging is sensitive to concentrations of contrast agent in a given region (related to perfusion), while T2*-weighted imaging is sensitive to the loss of compartmentalization of contrast agent (related to diffusion) (11). Our intent was to develop a technique combining both dynamic T1 and T2* signal intensity measures to gauge myocardial perfusion and diffusion simultaneously to achieve a more accurate assessment of viability.

# 2. Background information

## *2.1. Myocardial Physiology*

Myocardial metabolism depends on three major substrates to maintain myocyte function and viability; glucose, lactate, and free fatty acids (17). Under normal conditions, there is a preference for the aerobic generation of adenine triphosphate (ATP) from non-esterified fatty acids (18). This reliance places an $O_2$ demand of approximately 8-10 mL per 100 g of tissue per minute at rest, which may increase up to 300% during exercise (17).

To meet these requirements and maintain continuous function, the heart has developed an extraordinary system of blood vessels. The network originates from the base of the aorta and extends two large arteries to feed the left and right ventricles, known as the left and right coronary arteries. They run down the surface of the heart to the apex, continually branching off into smaller vessels (Figure 1).

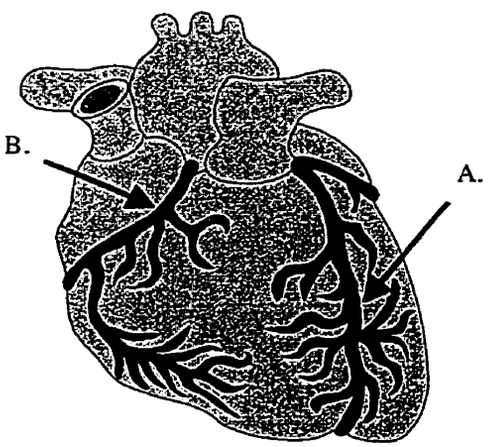


Figure 1. The coronary circulation of the heart is composed of two major vessel systems.
A. Left anterior descending coronary artery.
B. Right coronary artery.

Coronary vessels can be divided into two classes, small resistance arterioles and larger conductance arteries. It is the coronary arterioles that branch off until capillaries are formed. In a normal heart, there are nearly 2500 capillaries per cubic millimeter or one for each myocyte (19). Most cases of heart disease that lead to acute myocardial infarction (AMI) are due to a failure in the coronary circulation (20).

## Cardiac metabolism

Under normal conditions, the network derived from the coronary vasculature will adequately provide the myocardium with substrates and oxygen to fuel oxidative phosphorylation and maintain the heart. This is remarkable, as an estimated 4-8% of the total ATP is consumed during each contraction (21). The pool is replenished by a combination of anaerobic glycolysis, but more importantly, oxidative phosphorylation.

### 1) Anaerobic Metabolism

In 1907 Locke and Rosenheim observed glucose uptake in the isolated heart (18). Glucose is transported from the extracellular space into the individual myocytes by a process involving an insulin sensitive transporter (22). Once internalized, glucose can be used to produce ATP in a "fast" reaction that may be augmented through increased glucose uptake by facilitated diffusion or by regulation at the enzyme level (i.e. allostery) (22).

In healthy individuals the intracellular glucose concentration is low relative to the extracellular compartment (18). This provides an advantageous gradient and allows glucose, as well as other similar sugars, entry into the cell through carrier-mediated

facilitated diffusion (22-24). Insulin regulates this process; increased levels of the hormone will increase glucose transport. Additionally, high levels of insulin have been shown to increase the activity of hexokinase II and phosphofructokinase, the two regulatory enzymes involved in the metabolism of glucose (22).

For carbohydrates to be utilized, a conversion step is required to synthesize the 6-carbon sugar known as glucose-6-phosphate (G-6-P). Hexokinase II moderates this reaction, but requires that at least one ATP be hydrolyzed and converted to ADP (22-24). Once in the G-6-P form, enzymes in the cytosol lead to its rapid conversion into two, 3-carbon pyruvate molecules for a net production of 2 ATP and 2 NADH (22-24). The overall reaction may be summarized by the following equation:

$$\text{Glucose} + 2NAD^+ + 2ADP + 2P_i \rightarrow 2NADH + 2\text{pyruvate} + 2ATP + 2H_2O + 4H^+$$

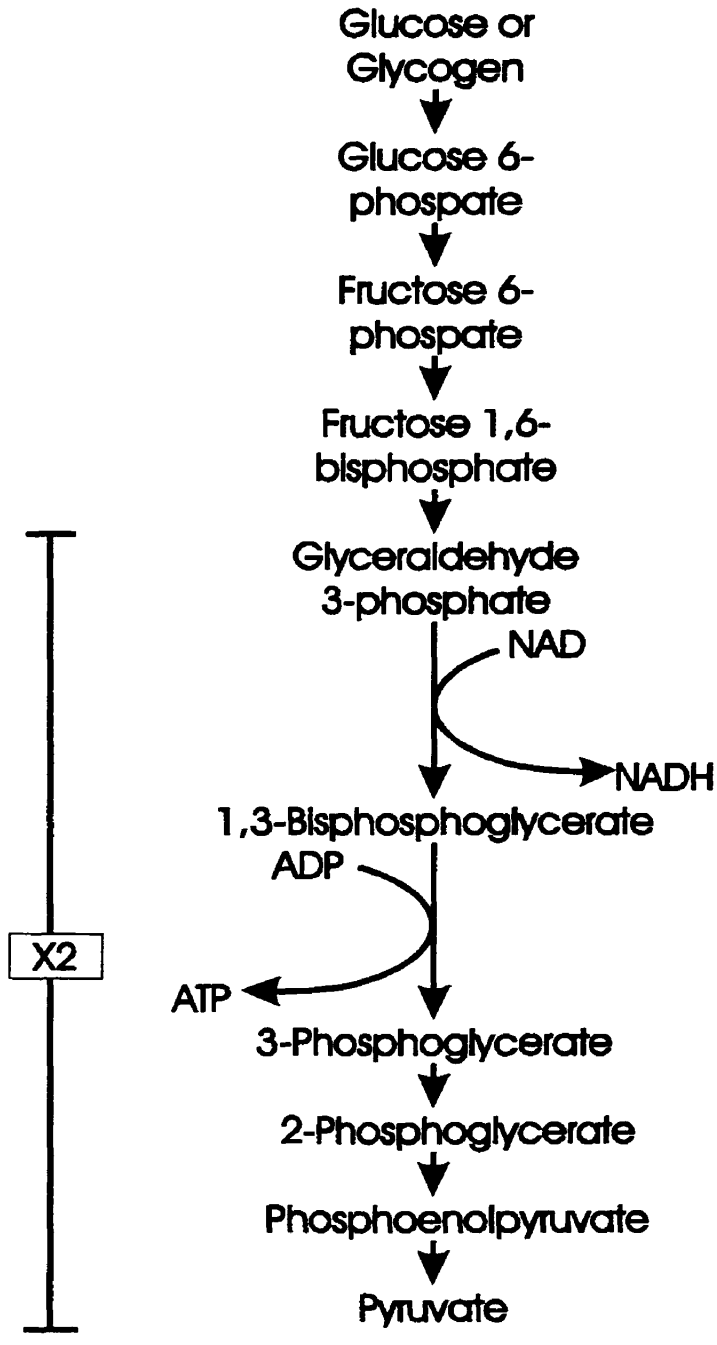


Figure 2. The glycolytic pathway, detailing the conversion of glucose or glycogen to pyruvate. (adapted from Lehninger AL, *et al.*, 1993 [23])

**2) Aerobic metabolism**

Oxidative phosphorylation is a relatively slow reaction that can be divided into two stages, the catabolism of acetyl-CoA through the citric acid cycle (also called Krebs cycle) and the generation of a proton gradient in mitochondrial respiration (18).

In the first stage, energy-rich substrates are converted to acetyl-CoA and oxidized through the citric acid cycle (25, 26). Because there are several reaction mechanisms to convert organic compounds to acetyl-CoA, the cycle may be considered the common pathway for the final metabolism of carbohydrates, lipids, and proteins (27). Essentially, the Krebs cycle reactions take a two-carbon acetyl-CoA and a four-carbon oxaloacetate, which combine to form citrate. Then in the series of steps that follow, two molecules of $CO_2$ are released and oxaloacetate is regenerated (25, 26). In one turn of the cycle there is one ATP equivalent in the form of guanosine triphosphate (GTP) created through substrate level phosphorylation, as well as three of the $H^+$ and electron equivalents nicotinamide adenine dinucleotide (NADH) and one flavin adenine dinucleotide ($FADH_2$) (25, 26).

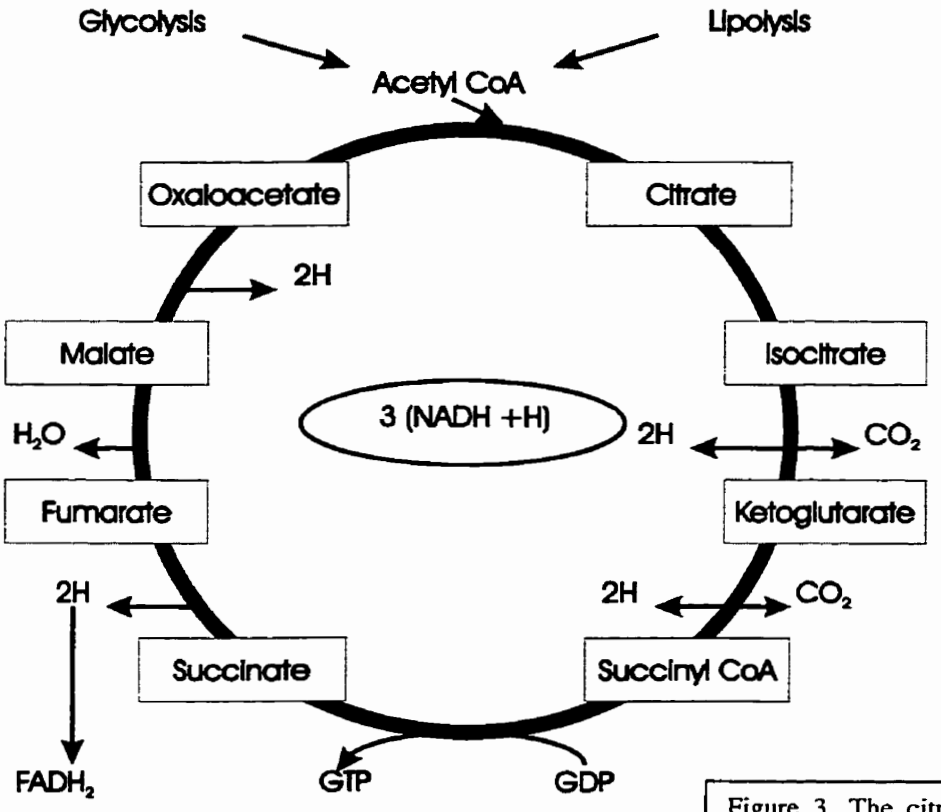


Figure 3. The citric acid cycle (adapted from Lehninger AL, *et al.*, 1993 [25])

Very little ATP is actually produced via the citric acid cycle. Under normal conditions, the majority of aerobic ATP is generated through the next stage of oxidative phosphorylation, which is mitochondrial respiration, or the electron transport chain. This step utilizes the NADH and $FADH_2$ that was synthesized during glycolysis and the citric acid cycle to generate ATP (28).

During mitochondrial respiration, there is a consumption of molecular oxygen, which is eventually reduced to $H_2O$. This allows the passage of electrons from NADH and $FADH_2$ to cytochromes b, c, and a through the mitochondrial membrane complexes I, II, III, and IV (25, 29). Each of these complexes is composed of membrane proteins that

are associated with redox-active prosthetic groups and increasing reduction potentials. An important feature is that complexes I, III, and IV function to "pump" $H^+$ ions to the intermembrane space of the mitochondria (25). This buildup of protons in the intermembrane space creates an electrochemical gradient that is used by complex V, also known as ATP synthase. ATP synthase uses the proton gradient to generate ATP via the exergonic return of $H^+$ into the matrix (25, 28, 29) (Figure 4).

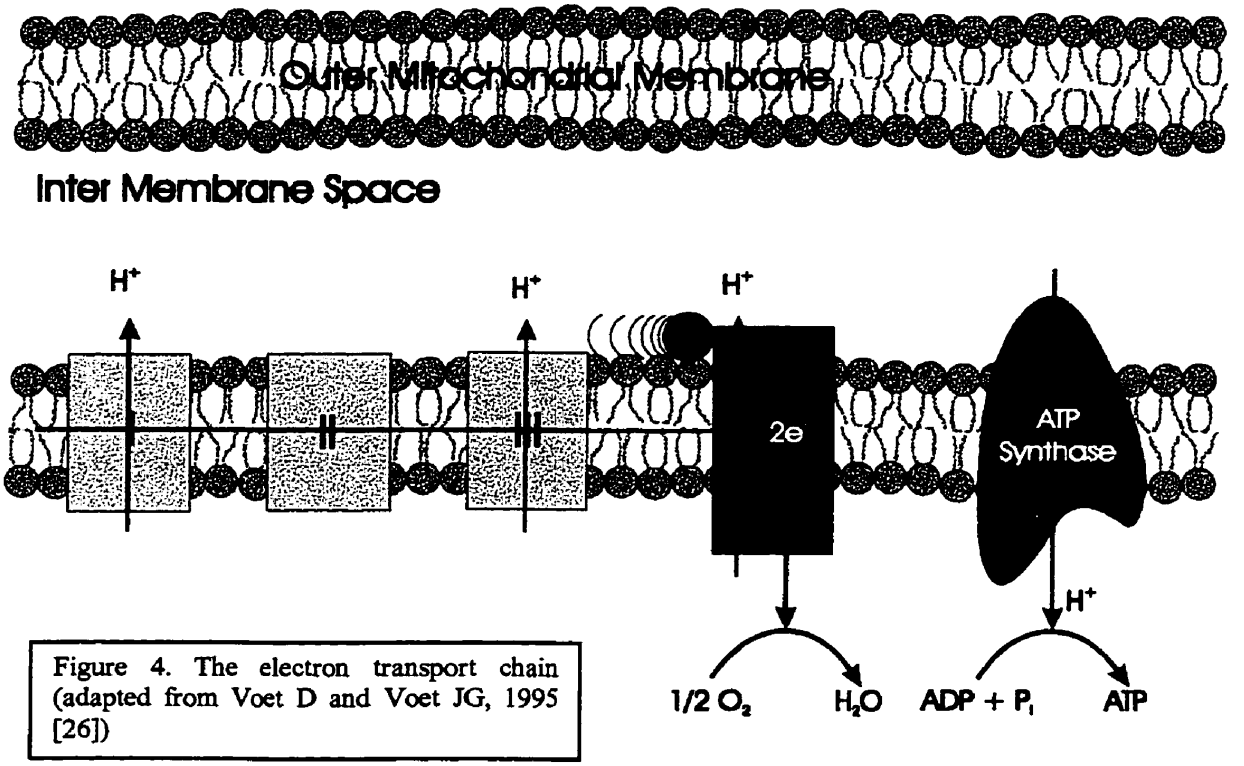


Figure 4. The electron transport chain (adapted from Voet D and Voet JG, 1995 [26])

**3) Substrates**

The normal heart can utilize a number of compounds to generate the necessary ATP to drive contraction. The most important of these are carbohydrates and fatty acids, which will be focused on. However, when necessary, amino acids and ketone bodies may also be used upon conversion to acyl esters and entry through the citric acid cycle (18).

*i. Carbohydrates*

Energy from carbohydrates is of less importance to the heart than oxidative phosphorylation. However, it is linked to the citric acid cycle, by the production of pyruvate and lactate, which can be converted to acetyl-CoA and oxidized through the citric acid cycle. It also produces 2 NADH during glycolysis, which may be consumed by the electron transport chain (22).

An important feature of carbohydrates as fuel sources is that they may undergo anaerobic glycolysis. Glucose can enter the cell by an energy neutral process of facilitated diffusion to be used for glycolysis. Also, cellular glycogen, which is normally present in small amounts, may also be converted to G-6-P during periods of reduced $O_2$ availability, such as ischemia. The myocardium becomes much more dependent on these forms of energy production, particularly glucose, when glycogen stores are depleted and glucose transport proteins translocate to the cell membrane (17, 18).

*ii. Free fatty acids*

Saturated free fatty acids (FFAs) are the heart's preferred substrate (18). To be utilized, they must first be transported into the mitochondria. Enzymes present on the outer mitochondrial membrane facilitate this process by esterification with a CoA-SH to yield a fatty acyl-CoA (26). Once converted to a fatty acyl-CoA, it is possible for the carnitine shuttle to transport it into the mitochondria. Here the acyl-CoA will undergo steps leading to β-oxidation to acetyl-CoA (25).

β-oxidation is a four-step process that yields energy equivalents in the form of NADH, in addition to those generated by the oxidation of acetyl-CoA. This makes saturated fatty acids a very rich energy source. The process of β-oxidation begins with the creation of a double bond between the α and β carbons of a saturated fatty acid, which is catalyzed by the acyl-CoA dehydrogenase enzyme (25). Acyl-CoA dehydrogenase is itself an electron carrier, by virtue of its FAD prosthetic group. Once the enzyme has catalyzed the reaction to create a *trans*-$\Delta^2$-enoyl-CoA. It will transfer the captured electrons directly into the electron transport chain via the electron-transfering-flavoprotein (ETFP) of the inner mitochondrial membrane (27). The second step results in the addition of a water molecule at the double bond by enoyl-CoA hydratase (26). Thirdly, β-hydroxyacyl-CoA dehydrogenase dehydrogenates the molecule using $NAD^+$ as the electron acceptor (25). Lastly, acyl-CoA acetyltransferase promotes the removal of a two-carbon fragment from the newly formed β-ketoacyl-CoA to create an acetyl-CoA (25). The process may then repeat itself until the entire fatty acid is oxidized to acetyl-CoA.

In summary, using a palmitoyl-CoA (with a 16-carbon backbone) as an example, the reaction would be as follows:

Palmitoyl-CoA + 7CoA +7FAD +7$NAD^+$ +7H2O → 8acetyl-CoA + 7FADH2 +7NADH +7$H^+$

## Myocardial Ischemia

The heavy reliance of cardiac tissues on aerobic metabolism implies that there will be severe consequences to ischemia (a decrease in oxygen supply that results in failure to meet the global or regional $O_2$ demands of the heart). This was elegantly shown in pioneering experiments performed by Tennant and Wiggers where it was observed that tying off a coronary artery would immediately lead to cessation of function in the region of myocardium fed by the vessel (30). These effects can be explained by changes in myocardial metabolism and function.

### 1) Myocardial metabolism during ischemia

During ischemia an imbalance develops between energy producing mechanisms and energy consuming processes. This imbalance is due to the decrease in high-energy phosphates produced by oxidative phosphorylation and the greater dependence on less efficient anaerobic glycolysis (31).

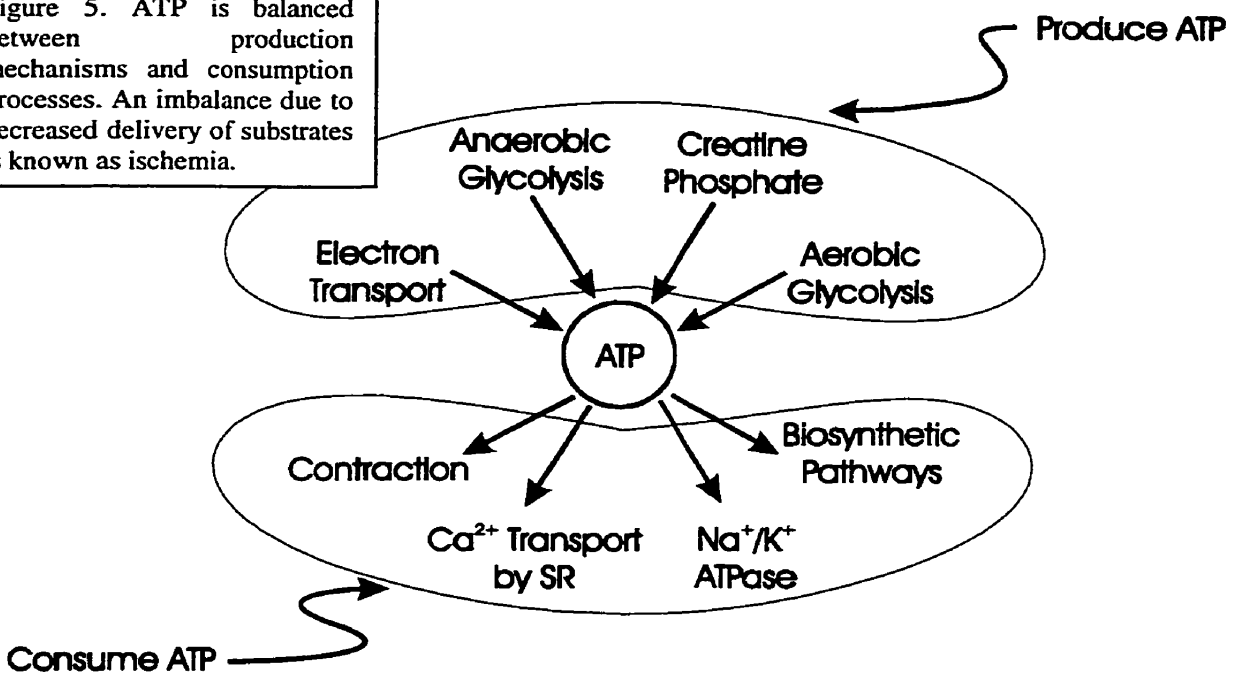


Figure 5. ATP is balanced between production mechanisms and consumption processes. An imbalance due to decreased delivery of substrates is known as ischemia.

With the loss of oxidative phosphorylation and following depletion of the glycogen pool, glucose becomes the primary substrate for ATP production (18, 31, 32). Thus with moderate ischemia there is increased glycolytic flux that is mediated by increased glucose transport through the cell membrane as well as hexokinase and phosphofructokinase (PFK) activity (both moderate rate limiting steps in glycolysis) (18, 31, 32). Additionally, there is further metabolism of glycolytic metabolites. Normally following glycolysis, the citric acid cycle and the electron transport chain will oxidize pyruvate and NADH. However, under strictly anaerobic conditions, there is a buildup of these metabolites, which can lead to the inhibition of glycolysis. To prevent this, a further reaction occurs in the absence of aerobic metabolic pathways where NADH is reoxidized to $NAD^+$ by coupling to the reduction of pyruvate to lacate. Given adequate perfusion $NAD^+$ can be reused, while lactate may exit the cell into the blood stream (25).

In cases of severe ischemia glycolysis is inhibited (18). This is likely due to inhibition of the PFK enzyme by acidosis resulting from inadequate washout of lactate (32, 33). This enzyme regulation may be considered a protective mechanism. When washout is marginal, the cell acts to prevent further acidosis by decreasing the glycolytic rate and lessening the production of metabolic byproducts (33, 34).

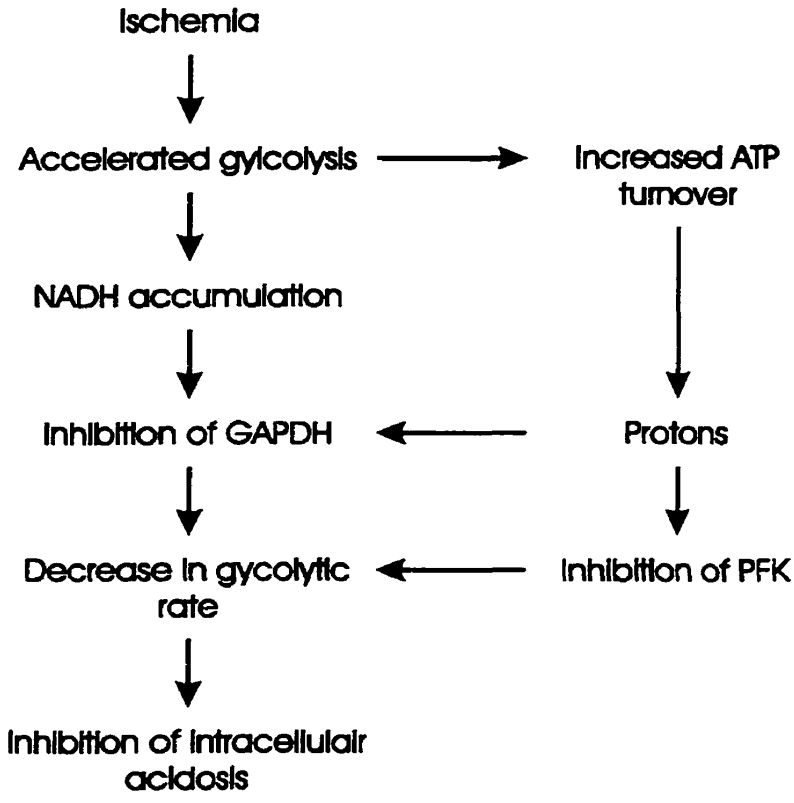


Figure 6. Regulation of anaerobic glycolysis during ischemia. (from Opie LH, 1995 [18])

**2) Ionic imbalance during ischemia**

The reduction in available $O_2$ has several immediate effects on the cell membrane that result in an increased resting membrane potential (35-37). A major factor is the inhibition of the energy-dependent $Na^+/K^+$ ATPase, which occurs in the early stages of ischemia (37). Failure of the $Na^+/K^+$ pump results in cascade of events that can lead to

cell necrosis. Acidosis and the lack of intracellular ATP are responsible for the decrease in $Na^+/K^+$ pump function. This alters membrane potentials due to increased intracellular $[Na^+]$ and extracellular $[K^+]$ in the vicinity of the sarcolemma (38). Membrane potentials are further disturbed by increased extracellular $[K^+]$ as it may cause the inactivation of rapid $Na^+$ channels (37, 38). Ion fluxes are augmented by the concomitant increase in $Na^+/Ca^{2+}$ exchange and activation of ATP-sensitive $K^+$ channels (39).

The aforementioned shifts affect myocyte function through a short-term decrease in the amplitude, duration, and conduction velocity of the cardiac action potential (AP) (38). However, the release of catecholamines during ischemia may stimulate slow $Ca^{2+}$ channels and cause a later prolongation of APs, which result in post-repolarization refractoriness and possible unidirectional block and reentrant arrhythmias (39).

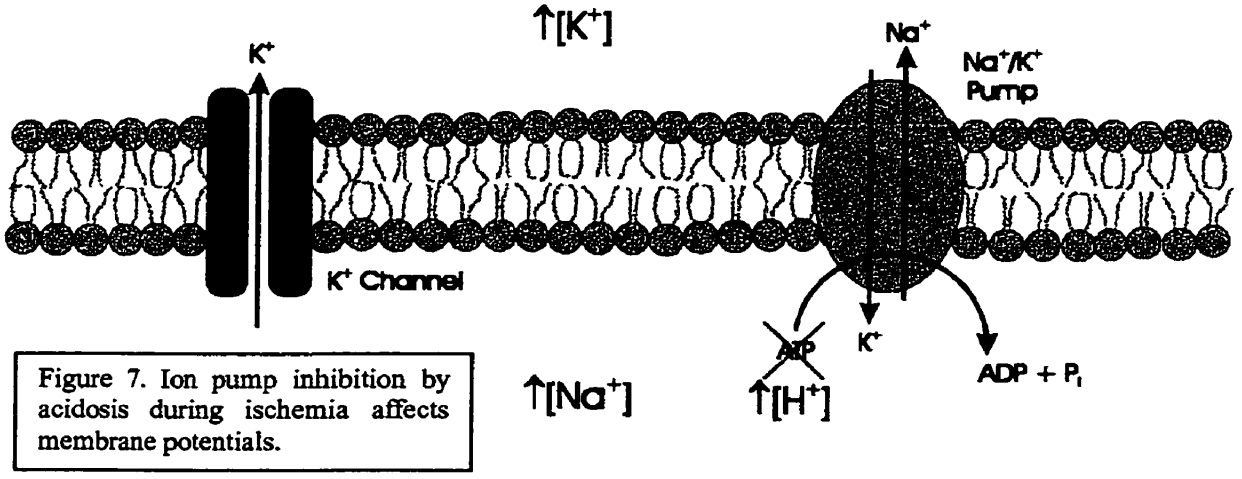


Figure 7. Ion pump inhibition by acidosis during ischemia affects membrane potentials.

Apart from the obvious electrophysiological effect, the slow inward $Ca^{2+}$ current is responsible for decreased myocyte contractility due to the abbreviation of the action potential plateau phase (39). Further, acidosis can cause decreased sarcoplasmic $Ca^{2+}$

release and uptake and further reduce contractile function via decreased myofilament sensitivity to calcium (39, 40). While detrimental, this may be a form short-term cardioprotection. The mechanical activity of the heart accounts for about 75% of the energy use under normal conditions. The inhibition of contraction may be considered a tradeoff for more available ATP to enable the maintenance of homeostasis and short-term survival during periods of marginal oxygen availability (40).

## Myocardial Infarction and Injury

When the decrease in myocardial blood flow is severe and/or prolonged, then irreversible damage or myocardial infarction will result. Typically, no single event leads to heart attack. However, AMI is commonly precipitated by the development of artherosclerosis in the coronary arteries, usually in conjunction with coronary thrombosis (40).

Whatever the cause, if the myocardium is reperfused before necrosis, aerobic metabolism will return to pre-ischemic levels (39). Failing timely reperfusion, hypoxia, acidosis, and the build-up of metabolites will occur. These ischemic changes cause immediate alterations in electrical activity, metabolism, and contractile function with the end result leading to necrosis.

### 1) Irreversible Injury

If blood flow to the myocardium is decreased to the extent where the myocytes are no longer able to maintain function, cell death may result. The region of the heart that is the most susceptible to severe ischemia is the subendocardium as this layer may require more oxygen (41). There is indirect evidence of this in the form of a higher capillary density in the region. But it is also known that endocardial tissue has a lower oxygen tension, which may cause a lower oxygen uptake, and a more anaerobic metabolism (41). When flow is reduced, this can lead to a greater depletion of ATP and creatine phosphate.

Once subendocardial ischemia has occurred, concomitant left ventricular failure causes compression on the coronary arteries and leads to an advancing wavefront pattern of tissue damage (41). Because of increasingly poor blood flow, more tissue becomes

involved, eventually encompassing epicardial zones (41, 42). Irreversible injury to the subendocardium generally begins at about 40-60 minutes of ischemia, while transmural infarction is present at 3 – 6 hours (41).

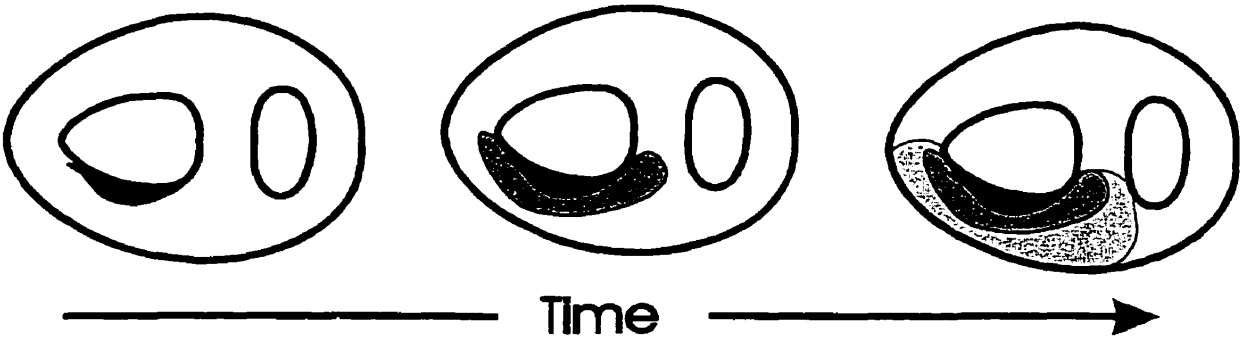


Figure 8. Progression of Infarcted Zone Following LAD Occlusion (adapted from Reimer KA, *et al.*, 1981 [42])

The key event differentiating reversible from irreversible injury appears to be the loss of cell membrane integrity (43, 44). Depletion of ATP and accumulation of toxic metabolites disrupt key ionic pumps resulting in the loss of the cell's ability to maintain biochemical and electrical gradients and leads to membrane damage (40). Increasingly severe ischemia results in the production of amphipathic catabolites of membrane phospholipids (45). In addition to damaging cell membranes, these can lead to the production of lysophosphoglycerides and long-chain acylcarnitines, which induce delayed afterpotentials and promote lethal ischemic arrhythmias (45).

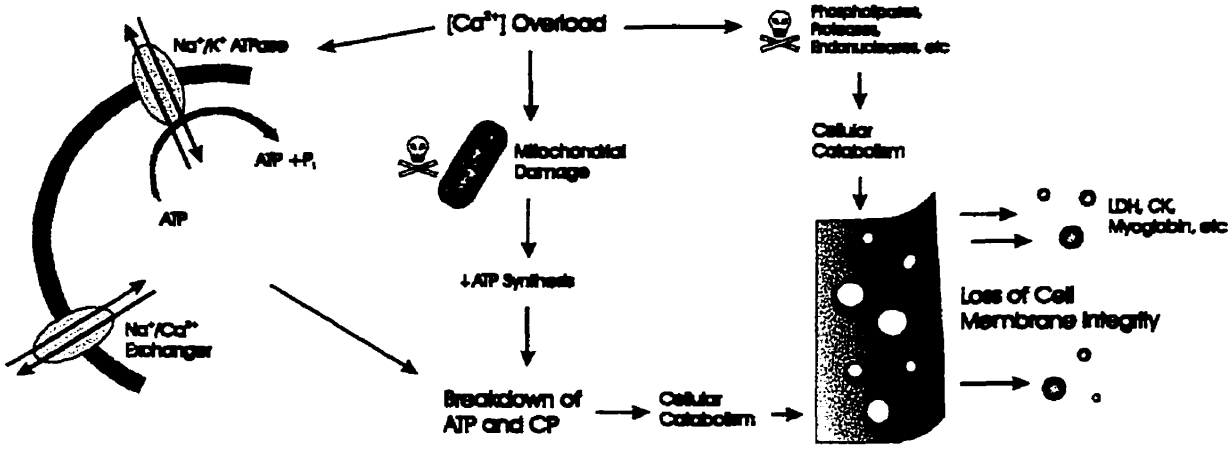


Figure 9. Depletion of ATP and ionic changes during ischemia can lead to infarction. This results in necrosis and a loss of cell membrane integrity (adapted from Fleckenstein –Grun G, 1994 [46])

Because cell membrane disruption is associated with necrosis, creatine kinase, lactate dehydrogenase, myoglobin, and aspartate aminotransferase leakage into the bloodstream are used as markers of membrane disruption and cell death (43, 44). Conversely, dye uptake into the intracellular space resulting from the same cell membrane degradation, has been used to identify nonviable tissues.

**2) Reperfusion injury**

Uncontrolled reperfusion, which can lead to the no-reflow phenomenon, ischemic cell swelling, and acceleration of myocyte necrosis or dysfunction, has been shown to result in injury beyond what can be attributed to ischemia (39, 40).

It is unclear what mediates reperfusion injury. However, there is a huge rise in intracellular $Ca^{2+}$ levels following reperfusion, which is particularly evident in the mitochondria. These cellular $Ca^{2+}$ fluxes are accompanied by myofibrillar disruption and

cellular edema (46). There is also fundamental injury by lipid peroxidation from oxygen-derived free radicals (47). Reactive oxygen intermediates (ROIs) may be the metabolic byproducts of the ischemic/postischemic cell or may be derived from neutrophils, which accumulate in the ischemic area following reperfusion (47). Both may be potent factors in the development of reperfusion injury (Figure 10).

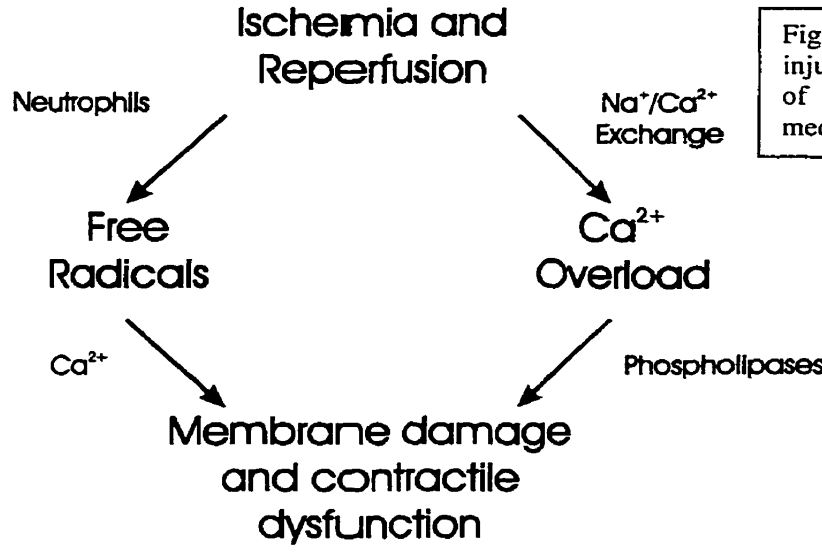


Figure 10. Reperfusion injury may be composed of $Ca^{2+}$ and free radical mediated damage.

*i. Calcium Overload*

Calcium ions have been chosen to play a central role in modulating the contractility of the heart. Under normal circumstances the level of free cytosolic $Ca^{2+}$ is kept at a low level by cell sequestration mechanisms. Calcium becomes toxic at high concentrations (48). Therefore a loss of homeostasis could be detrimental to the function of the myocardium. Calcium affects cell function in two ways; it can reduce myocyte contractility, but may also cause damage (48, 49).

During ischemia there are changes in the interactions with proteins involved in sequestration and/or contractile machinery (50). Mechanisms such as acidosis or the release of lipases may modify the phospholipid membranes of the cell (50, 51). If this happens at the sarcolemma, it affects the cell's ability to sequester calcium. The resulting increase of free cytosolic calcium could lead to the activation of protein kinases and affect the phosphorylation of contractile proteins, which in turn, can decrease the calcium sensitivity and/or the maximal $Ca^{2+}$ activated force (50, 51).

Ischemia is also associated with a depletion of ATP stores, which prevents the function of the $Na^+/K^+$ exchanger (52, 53). This influx of $Na^+$ acts to elevate intracellular $Ca^{2+}$ by increasing $Na^+/Ca^{2+}$ transport (53). Lower ATP stores also create difficulties in sarcoplasmic uptake and cellular extrusion of calcium ions (54). The elevated $[Ca^{2+}]$ causes a mitochondrial calcium overload, which can further reduce ATP production and cause damage to phospholipid membranes through the activation of phosphlipases (52-54).

*ii. Free Radicals*

Free radicals are formed via several biological reactions. Under normal conditions their reactivity is quenched by endogenous protective systems within the cell (such as enzyme catalysis) (47). Without these mechanisms in place, free radicals will interact with a variety of biological compounds (including lipids, proteins, DNA, etc) and can lead to cellular damage (lipid peroxidation, radical polymerization) (47, 55). Two of the most biologically important species of free radicals are the superoxide ($*O_2^-$) and

hydroxyl radicals (*OH). The major sources of these free radicals during ischemia are (55, 56):

i. the xanthine oxidase pathway

ii. activated neutrophils

iii. the arachidonate cascade

iv. the accumulation of reducing equivalents during $O_2$ deprivation

v. autooxidation of catecholamines

vi. derangement of the electron transport chain leading to univalent reduction of oxygen in mitochondria

Damage from free radicals is non-specific, but some proteins (particularly ion regulating and E-C coupling proteins) may be more vulnerable than others as sulfhydryl groups on these molecules may be especially vulnerable to oxidation. For example, free radicals have been shown to inactivate the $Na^+/K^+$ pump directly (55).

## Reversible injury

Following reperfusion, there is often an element of reversible injury in addition to myocardial infarction. This component of myocardial dysfunction has been described in two major forms, stunned and hibernating myocardium (57). This was shown in the 1970s with experiments performed by Heyndrickx *et al.* Commencing after flow was restored from a reversibly occluded coronary artery, researchers noticed a prolonged contractile dysfunction that gradually returned to normal. This condition was termed "myocardial stunning" by Kloner and Braunwald (57). Shortly thereafter they also coined the term "chronic myocardial stunning" to describe another form of reduced function.

This was from clinical observation of patients suffering from chronic ischemia who displayed a chronic depression in contractility (58). Rahimtoola coined the more recent and common name for chronic stunning, "hibernating myocardium" (57).

Both stunned and hibernating myocardium are becoming increasingly important conditions for cardiologists (1-3). Periods of depressed function are common after surgery and pharmacological support is often required (1-4).

**1) Stunned myocardium:**

Stunned myocardium is a generic term used to describe the functional deficits seen in a wide range of experimental and clinical settings, some lasting hours, some lasting in excess of several months. There are two main hypotheses explaining the phenomenon of stunning (57, 58). The first is centered on the idea of calcium overload as the agent of dysfunction. In this view, stunning is due to increased intracellular calcium as it has detrimental effects leading to a decrease in $Ca^{2+}$ sensitivity and induced force (50, 59). The second hypothesis is the oxyradical hypothesis, which insists that reperfusion and the resultant flux of reactive oxygen species cause cellular damage leading to the observed contractile deficits (47, 56). Most likely though, the actual progression of stunning depends on components from both the overload and radical hypothesis. Stunning appears to be a multifactorial process that depends on a complex interaction of pathogenic mechanisms and cellular alteration.

**2) Hibernating myocardium**

Hibernating myocardium, as opposed to stunned myocardium, shows persistently impaired myocardial and left ventricular function following a reduction in myocardial blood flow (2, 60). It can occur during unstable angina, chronic stable angina, and myocardial infarction. Importantly, function is restored with an increase in myocardial perfusion and/or decrease in myocardial oxygen demand (2, 61). Another difference from stunning is that in hibernating myocardium, tissues appear to have lowered metabolism and energy requirements related to its decreased function (60, 61). These observations have brought out speculations of a "smart heart" or that hibernation is a protective mechanism that matches oxygen demands (via modulation of contraction) to that which the local perfusion is able to supply (60). While this may or may not be true, hibernation is receiving a considerable amount of attention from cardiac surgeons. In a clinical setting, hibernating myocardium may be considered a reserve of tissues that can be salvaged with revascularization (2, 4, 61). Complete or nearly complete recovery of function can be expected when therapeutic intervention is received in a timely fashion (2, 61). Unfortunately this protection is limited. While hibernation can prevent ischemic symptoms and necrosis, myocardial $O_2$ demands may exceed the limits of what can be tolerated. This leads to progressive subcellular damage and/or necrosis (59) emphasizing the need for accurate diagnosis and prompt treatment.

## 2.2. Nuclear Magnetic Resonance

### Basic Principles

Nuclear magnetic resonance is made possible by a physical property of protons and neutrons known as spin. While there are two forms ("up" and "down"), it is important to understand that protons and neutrons tend to group themselves in spin-opposed pairs (62) (Figure 11).

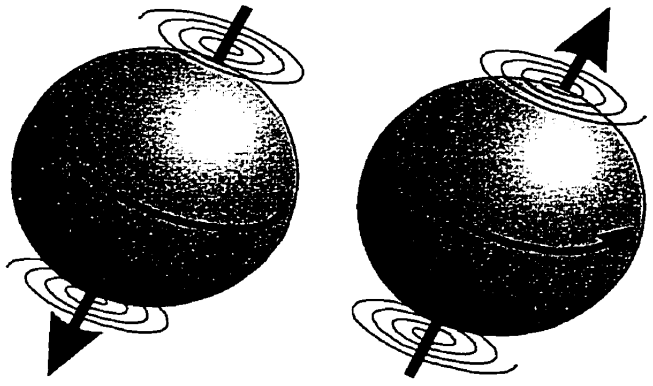

Figure 11. Particles such as protons and neutrons tend to pair with one particle in an "up" orientation and the other in a "down" orientation.

This cancels out the effects of spin in many atoms (62, 63). But some nuclei possess an uneven number of protons or neutrons (such as in $^{1}H$ and $^{31}P$) and there are unpaired particles. Because nuclear spin attributes to the particles an angular momentum vector and a magnetic dipole moment, these nuclei behave like tiny bar magnets (Figure 12) (64, 65).

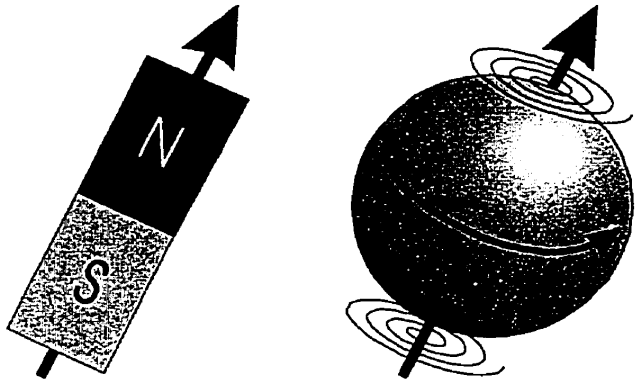


Figure 12. A lone unpaired particle can have magnetic properties due to spin.

**1) The Proton**

NMR can be most easily described using the example of the hydrogen nucleus, which is composed of a single proton. A lone proton possesses an intrinsic spin and mass, and therefore a spin-angular momentum (62, 63). But because a proton also possesses a charge, there is a magnetic dipole moment (64, 65). The magnetic properties of hydrogen go unnoticed as the nuclei around us are subject to thermal motion and they are continually reorienting themselves. This results in a averaging of their magnetic effects (65).

In NMR the magnetic dipoles are manipulated using a static magnetic field, conventionally termed $B_0$. This is applied to alter the random orientation of the protons. Normally there is no reason for a proton to align in any particular direction, but when placed by a magnet, alignment with the field becomes more favorable energetically (65). A hydrogen nucleus may take one of two orientations, one where the magnetic dipole moment is parallel to the field and one where it is anti-parallel (65, 66). Because the parallel orientation is favored, a disproportionate number of protons become aligned and leads to a small, but important net magnetization vector (called M, which is the sum of all the individual magnetic vectors within the sample) is created (65, Figure 13).

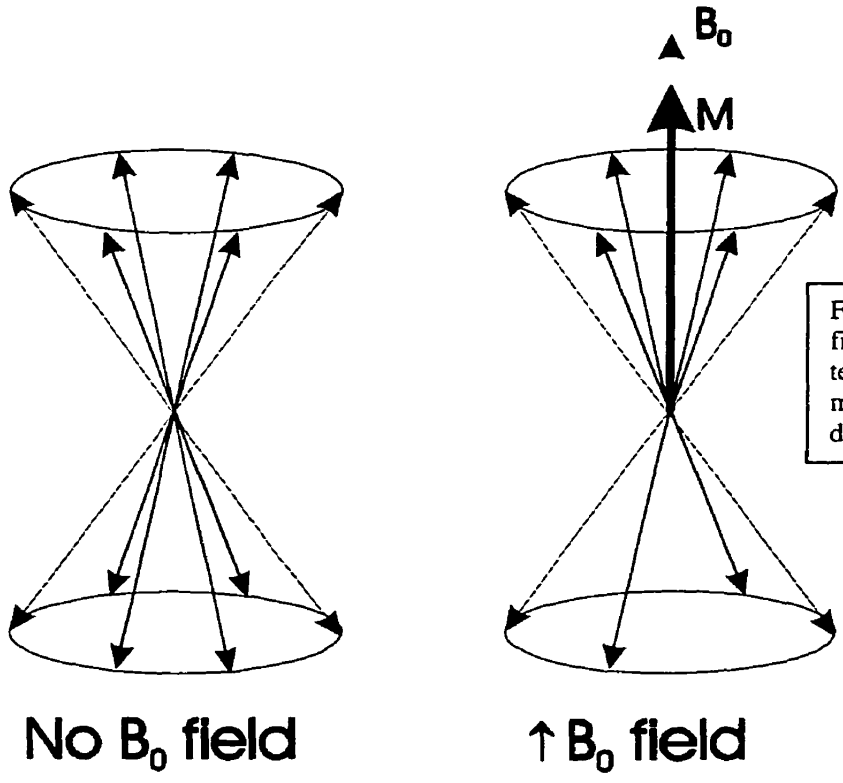


Figure 13. In a strong magnetic field, individual dipoles will tend to align leading to a net magnetization (M) in the same direction as $B_0$.

From Figure 13, it is apparent that it is the net magnetization that aligns with the $B_0$ field and not the magnetic dipoles. This is because protons possess a spin angular momentum and when exposed to a static magnetic field they do not align parallel to the field *per se*, but the angular momentum vector will precess around the direction of magnetic field lines (67). This motion is known as precession and it occurs at a specific frequency dependent on the strength of magnetic field (62, 66, 67). An analogous situation is the example of a spinning top (65). When you take a top and spin it, the top will eventually begin to wobble. This wobble occurs when the angular momentum is tipped away from the axis of the field and the motion is known as precession (Figure 14).

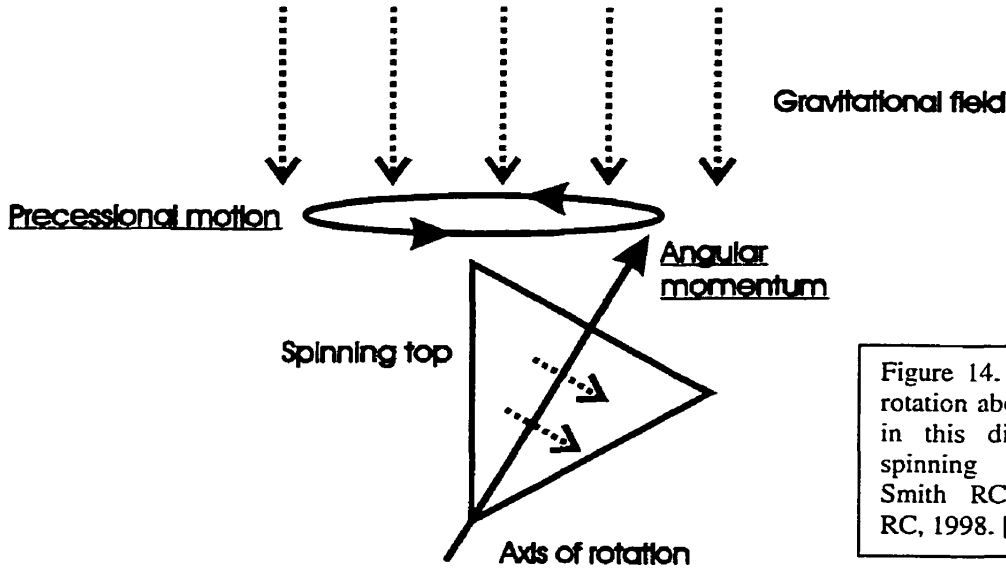


Figure 14. Precession is rotation about an axis as in this diagram of a spinning top. (from Smith RC and Lange RC, 1998. [65])

Protons behave similarly. Instead of a true "physical" spin, a proton has intrinsic angular momentum and a magnetic dipole moment that will tend to rotate about the $B_0$ field. The rate at which precession occurs is also known as its resonance frequency ($\nu$) and is proportional to the external magnetic field strength (67), related by the following equation:

$$\nu = \gamma B_0 \qquad (1)$$

where $\gamma$ (known as the gyromagnetic ratio) is a constant, specific to each species of magnetic nuclei and $B_0$ is the external field strength. The gyromagentic ratio of a proton is about 42.86 MHz/Tesla (63). Therefore, the resonance frequencies of protons in 1.5 and a 7 Tesla fields are equal to about 64 and 300 MHz respectively.

All magnetic nuclei in a sample, such as $^{1}H$, $^{31}P$, $^{11}Na$, etc will precess at their own distinct resonant frequencies in a static $B_0$ field. Therefore it is possible to alter the orientation of the net magnetization vector for one specific type of nucleus. This is achieved by the application of a secondary magnetic field ($B_1$) at the resonant frequency

of the nuclei of interest (67). Because each species of nucleus precesses at its own frequency, oscillating the $B_1$ field at the same rate will result in resonance (66). The secondary field will effectively alter the magnetic field experienced by the nuclei it is in resonance with and lead to a tipping of the net magnetization into the x-y plane (66, 67).

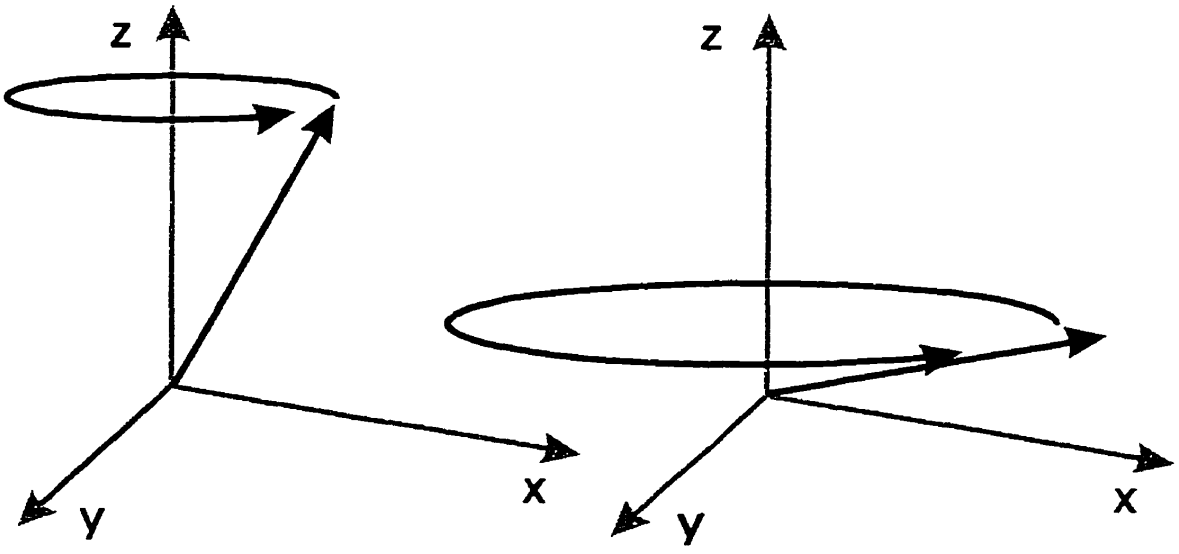


Figure 15. Resonating a $B_1$ field will cause the net magnetization to dip into the x-y plane due to the precession of individual protons.

## Magnetic Resonance Spectroscopy

Magnetic resonance spectroscopy (MRS) is a very powerful, non-destructive tool that is suited to analyzing and quantifying both the chemical and local magnetic properties of a sample. With MRS it is possible to distinguish chemical compounds and

their contributions to a sample and thereby locate organic compounds and calculate the rates at which they are being used or created (68).

**1) Basics of MRS**

MRS requires that a sample (or subject) be placed in a strong magnetic field. Typically, a combined transmit/receive surface coil is then placed near the volume of interest. In the most basic case, this coil is used to generate a small magnetic field at the resonance frequency of a specific nucleus (68). This tips the magnetization of the nuclei precessing at the same frequency. Once the magnetization has tipped into the x-y plane, the nuclei in the sample are allowed to relax and reorient to the $B_0$ field (68). As this occurs, the coil can then be used to acquire a signal from the shifting magnetic field. Because the magnetization in the x-y plane rotates coherently in the plane, it will generate an electromotive force in the receiving coil (67). The current that is generated oscillates at the same frequency as the precessing nuclei. This signal is called a free induction decay (FID) and is analogous to a sonic wave (67). It is a set of frequencies in the time domain that represent resonating nuclei in the sample and can be converted from the time domain to the frequency domain by performing a mathematical procedure known as a Fourier transformation (66, Figure 16). In the frequency domain, the area under the curve is proportional to the number of nuclei present in the sample.

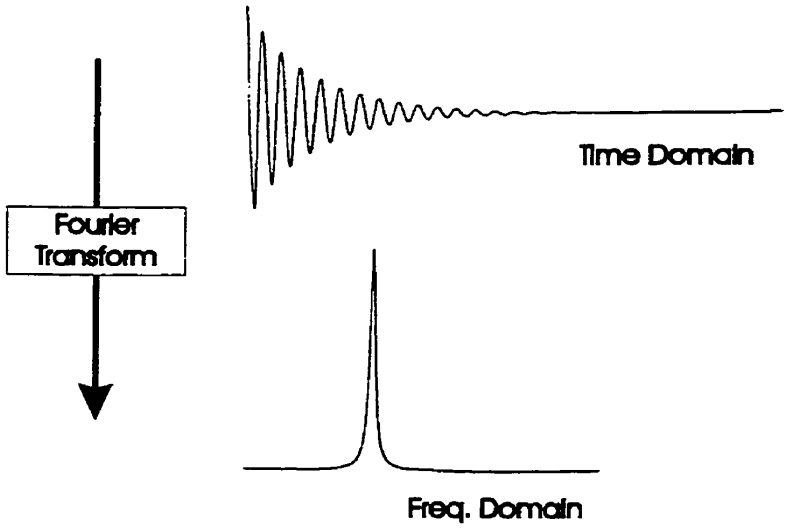


Figure 16. Free induction decay with conversion to frequency domain (adapted from Gadian DG, 1995. [66])

**2) Chemical Shift**

Conventional samples are very rarely homogeneous. In such cases, MR spectroscopy results in interactions of magnetic nuclei with other adjacent chemically different species and FIDs become much more complex than in our example. They will contain a range of frequencies that can be determined with the Fourier transformation. The distribution of frequencies is due to the local chemical or electronic properties. This phenomenon is known as chemical shift (68, 69).

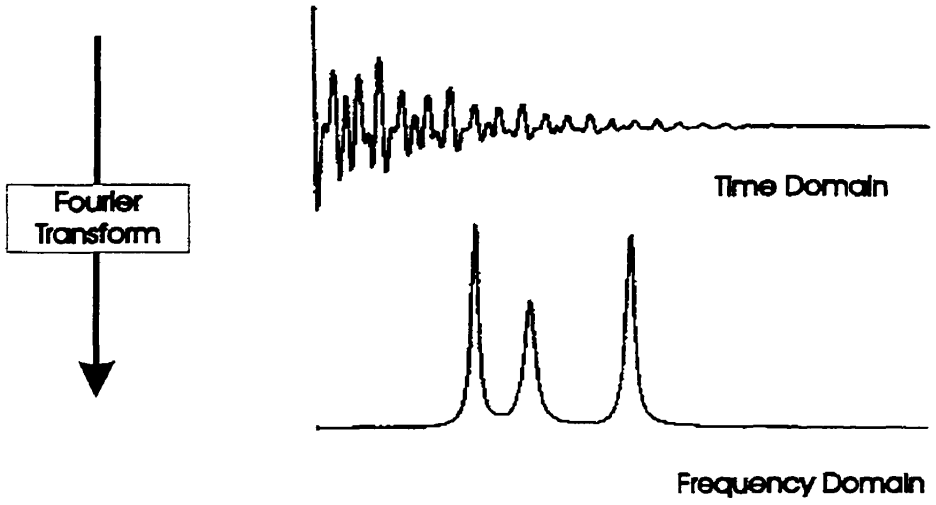


Figure 17. FT on an FID leads to transformation of data to a frequency domain.

Chemical shifts are due to inhomogeneities in the local magnetic field. One important source is from electrons (69), which are affected by factors such as electronegativity of a nucleus, conjugation of bonds, and resonance structures of the molecule. Electrons create magnetic fields that tend to act in opposition to the applied field, and result in the chemical shift due to the amount of shielding ($\sigma$) experienced by the nuclei (68, 69).

$\sigma$ is dependent on the chemical and electronic environment experienced by the nuclei. Different chemical environments give rise to different $\sigma$ values, which slightly alter frequency (69). This is extremely important to MR spectroscopy. It is possible to separate not only species of nuclei, but also the chemical nature of nuclei, based on the frequency (69). One example is of this use is to identify, by chemical shift, electronically differing species of the same nuclei (such as the $\alpha$, $\beta$, and $\gamma$ $^{31}$P of ATP, 70).

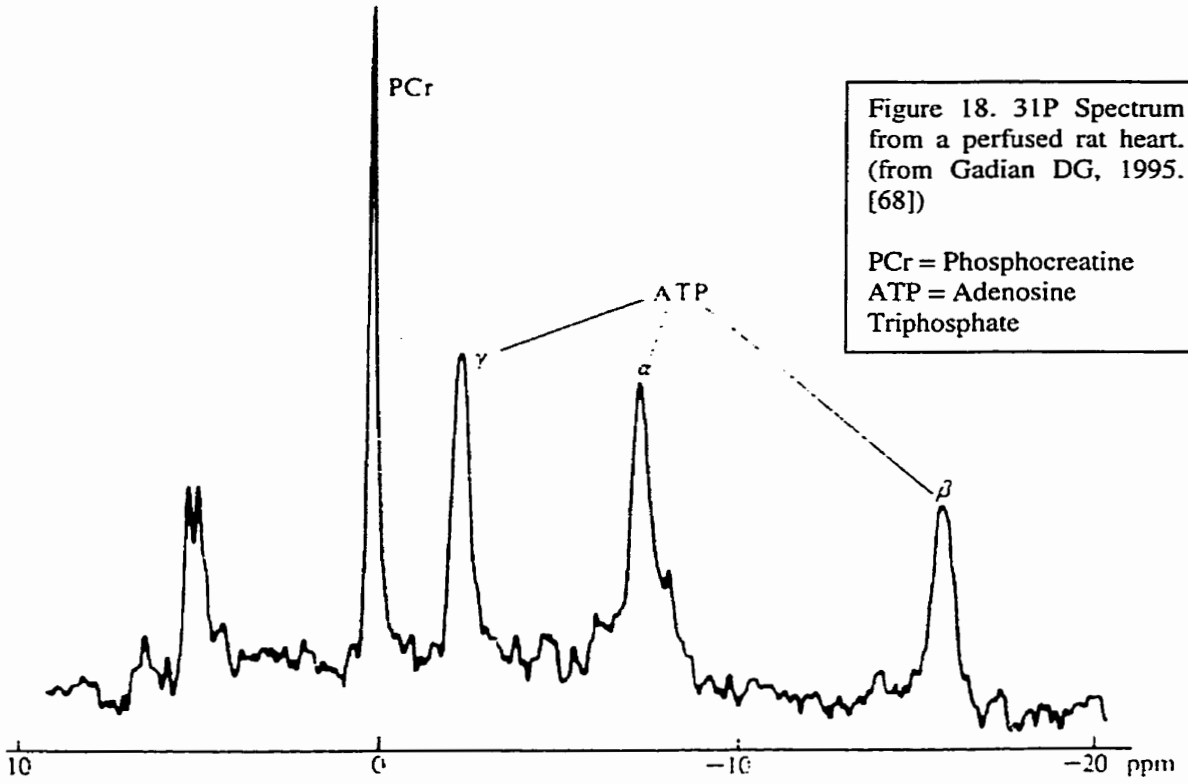


Figure 18. 31P Spectrum from a perfused rat heart. (from Gadian DG, 1995. [68])

PCr = Phosphocreatine
ATP = Adenosine Triphosphate

## Magnetic Resonance Imaging

Image data can be extrapolated from the RF signal generated by an MR experiment. However, sampling methods and data must be manipulated to acquire a 2 or 3 dimensional image.

### 1) Basics of MRI

The basic principle is straightforward and similar to magnetic resonance spectroscopy, but MRI takes advantage of the linear relationship between the strength of a magnetic field and the resonant frequencies of the magnetic nuclei (65). If the strength

of the $B_0$ field is altered according to distance along an axis you can relate the different resonant frequencies to position along the z-axis (71).

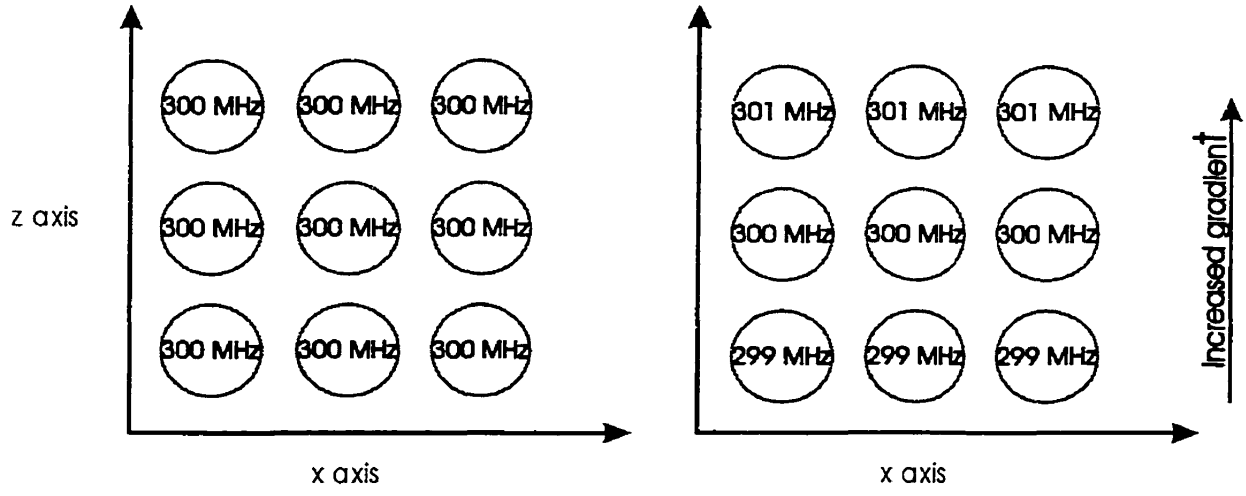


Figure 19. Application of a magnetic gradient along a direction leads to a spatial separation in frequency.

This is done using gradients, which are magnetic coils designed to produce an uneven field, which increases or decreases as a function of distance (72).

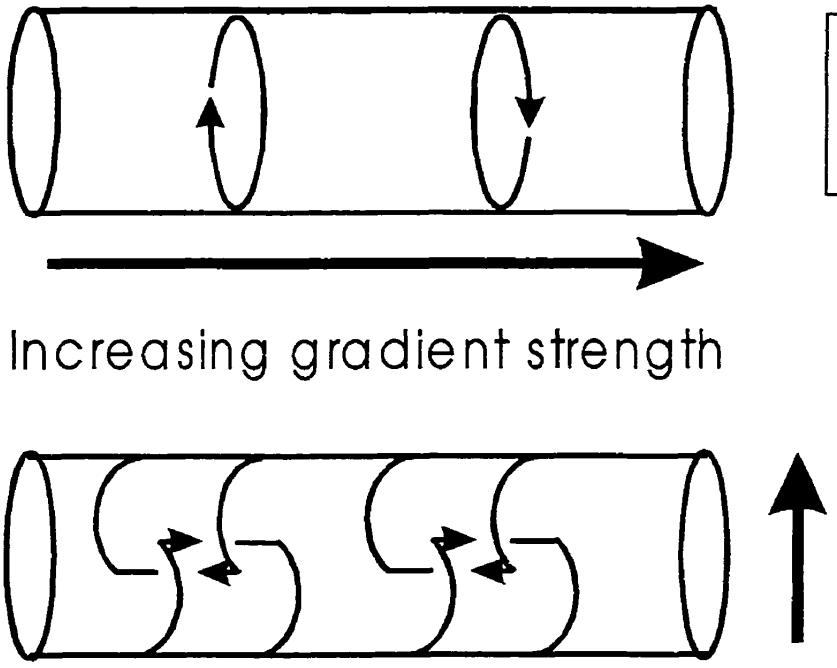


Figure 20. Examples of gradient coils used to create linearly variable magnetic fields for MR imaging. Maxwell pair (top) and Golay coils (bottom)

Three gradients are applied sequentially and data are acquired after each one. This process creates the desired spatially separated frequencies, but it also creates a separation in phase (71).

**2) Creating an image**

To reconstruct an image from the signal derived from an NMR experiment, the three magnetic gradients need to be applied in a specific order. This is typically shown schematically using a pulse sequence diagram (Figure 21).

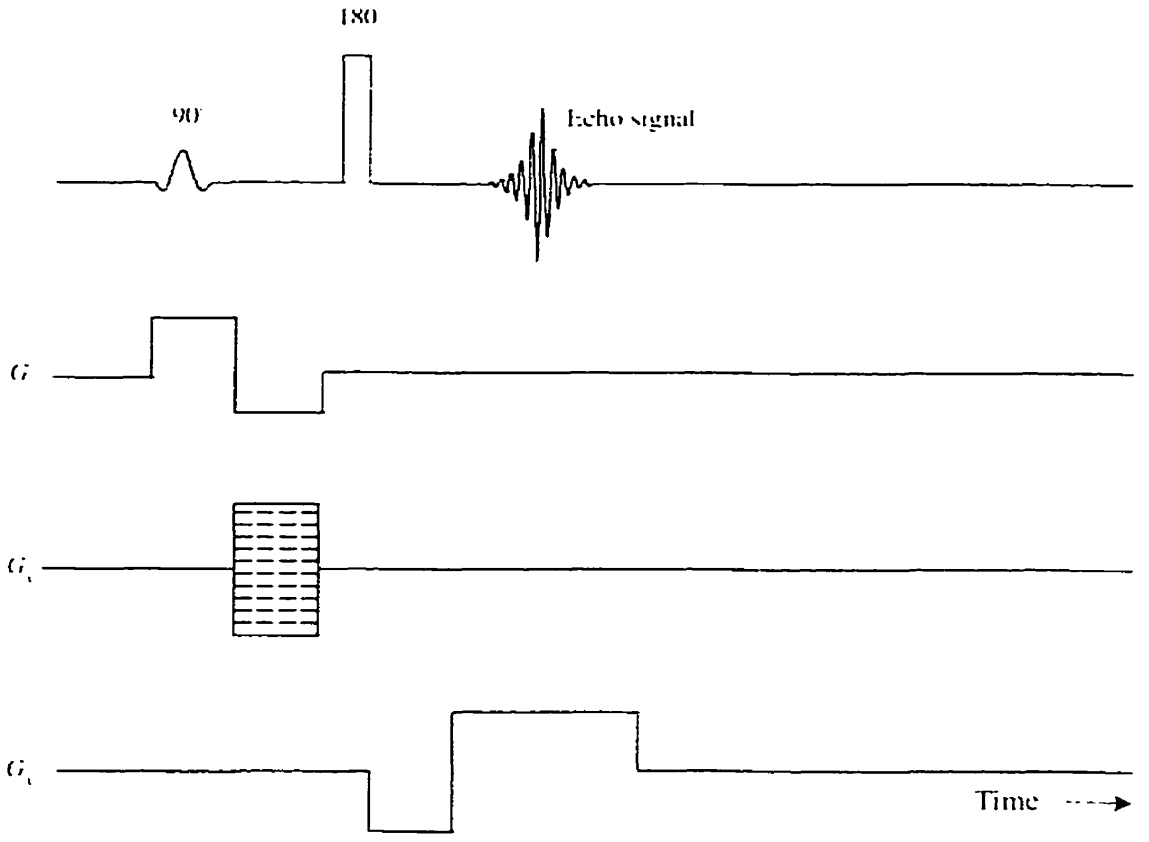


Figure 21. Spin Echo pulse sequence displaying the application of gradients to produce an image (from Gadian DG, 1995 [73]).

The three gradients shown in Figure 21 are known as the slice select ($G_z$), phase encoding ($G_y$), and the read ($G_x$) gradients. All three components help create a signal that is a composite of frequencies (relaying information along one axis, x) and phases (information along the other axis, y).

The slice select gradient selects a slice along a single axis. By applying the $G_z$ gradient, you alter the effective $B_0$ field strength in the z-direction (71). This causes the nuclei along the z-axis to precess at a different frequency from the other regions of the sample. By applying a $90^0$ pulse at the frequency related to a particular position, you can excite the nuclei in a specific region.

The phase encoding gradient is then used to acquire information along the y-axis. It temporarily alters the precessional frequency of the nuclei in the sample as a function of distance along the y-axis (71). By turning the gradient on before the signal reception processes, you alter the rate at which nuclei precess. But once the gradient is turned off, and nuclei are again precessing similarly, a phase shift will have been introduced (Figure 22). This process is repeated several times, leading to a number of sampling points along the y-axis. The gradient is manipulated so that it shifts from one direction to another. The numbers of gradient changes used to achieve the change in direction are known as phase encoding steps.

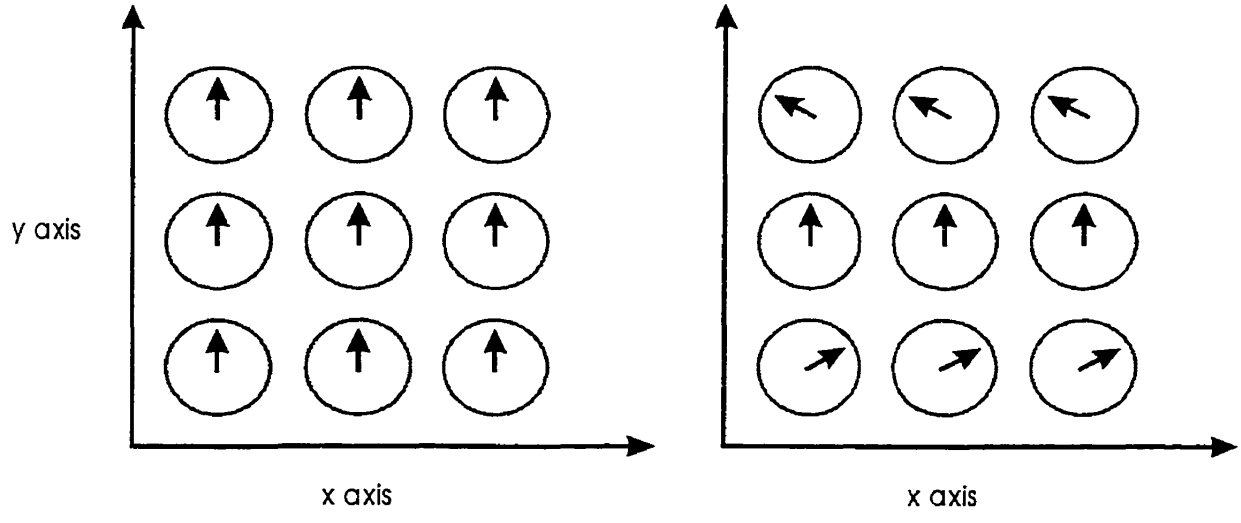


Figure 22. Phase encoding results in spatial separation of phase along the y-axis.

The final step is the application of a read gradient, which is applied during the signal measurement step to alter the frequencies in the sample. By introducing frequency

differences that correlate to distance along the read-axis it is possible to locate the signal component from any point along the axis by choosing the appropriate frequency (71).

Using the read gradient and sampling the phase-encoded signal at various points, data can be collected that possesses both phase and frequency components. Because phase and frequency are at right angles to one another, data is sampled into "k-space". This is essentially a real and imaginary number matrix that simplifies the calculations needed to construct an image from the data.

## Relaxation

MRI can develop image contrast based on proton density as well as on relaxation properties. The latter refers to the ability of the magnetic nuclei to absorb and release energy (72). In order to cause precession and have the net magnetization fall into the x-y plane, it is necessary to apply energy (with an oscillating $B_1$ field) to the protons in the sample. This leads to an unstable equilibrium. Once the $B_1$ field is eliminated, processes act to return the distribution of protons back to their equilibrium value within the $B_0$ field.

### 1) T1 and T2 relaxation

These relaxation mechanisms can be broken down into two components. Firstly magnetization returns to the z-axis. The process that is involved is known as longitudinal or spin-lattice relaxation and is characterized by T1 relaxation time. Secondly, magnetization will decay in the x-y plane. This process is termed transverse or spin-spin relaxation. This is characterized by T2 relaxation time (72). Both T1 and T2 relaxation times are measure of the time needed for the net magnetization vector (along the

longitudinal axis and the transverse planes respectively) to return to equilibrium in the $B_0$ magnetic field once the influence of the $B_1$ field has been removed. More precisely, T1 is the time needed for the longitudinal component of magnetization to recover to about 63% (or $[1-1/e^1]$) of its original value. And T2 is equal to the time needed for the transverse component of magnetization to return to about 37% (or $1/e^1$) of its original value in the absence of gross inhomogeneities (72). A third time measurement known as T2* is also used. This represents the observed T2 relaxation. Variations in the $B_0$ magnetic field cause the observed T2 to be shorter than would be expected due to an increased dephasing in the transverse magnetization of the x-y plane. The time constant that is seen is termed T2* to differentiate it from the actual T2. Because the homogeneity of the $B_0$ magnetic field will differ from magnet to magnet, T2* varies among NMR systems (73).

**2) Relaxation time weighting**

It is possible to skew image acquisition or to weight for T1 or T2* properties by modifying the timing of image acquisition. As shown in Figure 23, following a $90^0$ pulse the contributions of T1 and T2 relaxation to an MR signal is different, and will change with time. By modifying the moment at which data are acquired, it is possible to eliminate the signal contributed by longitudinal or transverse magnetization. This is useful as each these parameters can provide different information about the sample being examined. For example, due to the nature of spin-lattice relaxation mechanisms, T1-weighted images show high intensity where tissues contain large amounts of lipid and charged proteins (which bind to bodily fluids) (72). Alternatively, T2 and T2* images are good at observing flow phenomena since the compartmentalization (and oxygenation

state) of hemoglobin can increase the rate at which magnetic dipole moments dephase (73).

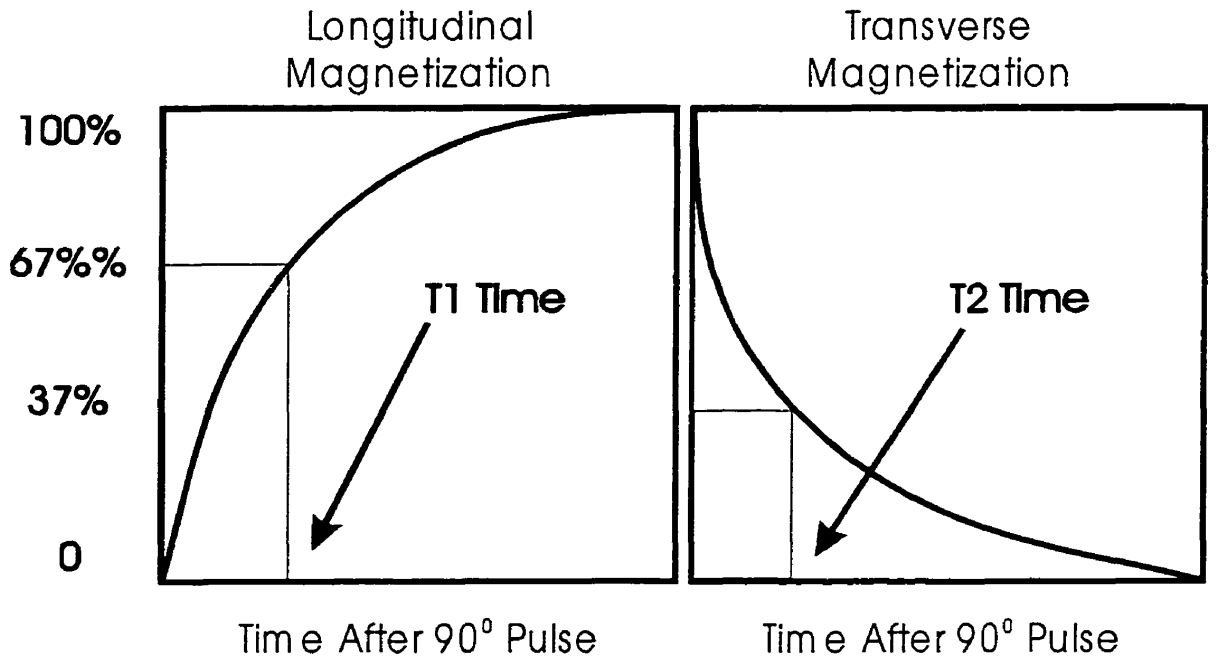


Figure 23. Relationship between time and recovery or loss of signal in T1 and T2* relaxation. Note that the time scale for T2 is typically much shorter than for T1. (adapted from Smith RC and Lange RC, 1998. [72]).

## Contrast Agents

In many situations, the differences between relaxation properties in tissues are minor (e.g. infarcted and viable tissue in the heart or brain). Ideally, what is needed is a compound that can perturb the tissues' relaxation times to increase the contrast between them. This has led to the development of various forms of contrast agents (74).

A contrast agent needs to influence the local magnetic properties of a sample and must therefore have strong dipole-dipole interactions (74, 75). These interactions may

affect T1 or T2* relaxation. Common forms of contrast agent are based on chelates of gadolinium (75). Gadolinium is a lanthanide metal that can be ionized in aqueous solution. When ionized, gadolinium becomes $Gd^{3+}$ and possesses seven unpaired electrons (76). This makes it highly paramagnetic and provides the strong dipole-dipole interactions needed in a contrast agent. However, ionic gadolinium doesn't normally have an effect on relaxation because $Gd^{3+}$ in solution is relatively small and tumbles rapidly (77), which prevents optimal interactions with surrounding protons. By chelating the ion to another molecule such as Diethylene Triamine Pentaacetic Acid (DTPA) this rotational speed is reduced. When tumbling closer to the resonant frequency of hydrogen nuclei its effects are greatly increased (77).

## 2.4 Magnetic Resonance Myocardial Viability Assessments

### Basics of MR assessments

Researchers have attempted to assess myocardial viability or infarction size using contrast enhanced MR imaging. A common technique is to probe for cellular injury, of which membrane damage is an important component (78, 79). This may be done by T1-weighted imaging techniques based on the assumption that a loss of cell membrane integrity increases the available distribution volume for contrast agent. The increased regional concentration leads to an increased regional MR signal and may be used to identify infarcted tissues. Because T1-weighted imaging is sensitive to the amount of contrast agent in a given region, and may be influenced by membrane damage, contrast-induced hyperenhancement is equated with non-viability (80-82).

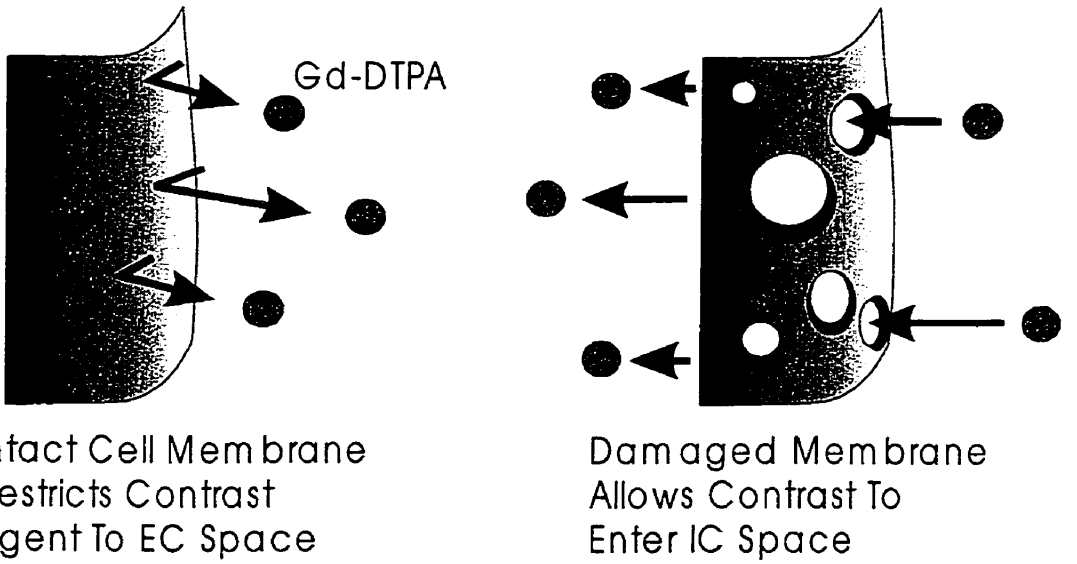


Figure 24. One effect of cell membrane damage is to allow contrast agent entry into the intracellular space (IC) from the extracellular space (EC).

In a study by Periera and colleagues, it was demonstrated that T1-weighted imaging in an infarcted canine heart model with a 2-hour coronary occlusion, leads to a significantly higher partition coefficient of Gd-DTPA in infarcted myocardium than in normal tissue (83, 84). They also found that the partition coefficient of the contrast agent was inversely related to $^{201}$Thallium uptake. This suggests that the distribution volume of a contrast agent is related to myocardial viability.

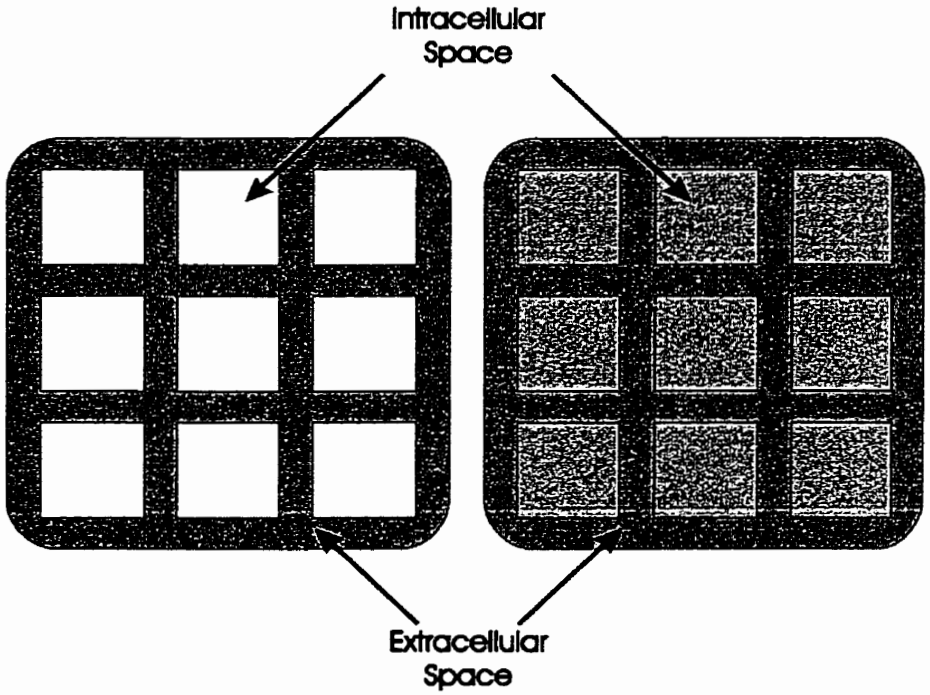


Figure 25. Entry of contrast agent into the intracellular space leads to an increased regional concentration of contrast agent (adapted from Nilsson S, 1995 [78]).

## Controversy

These findings have been somewhat controversial (85-87). A recent study from Higgins' group showed that the infarct size determined by Gd-DTPA enhanced T1 signal

intensity was significantly larger than that quantified by TTC staining (85). The overestimate area may be due to the presence of pleomorphic populations of viable and nonviable cells that can border the more easily defined infarcted region. Another reason may be interstitial edema, which is a common event in myocardial injury. Edema can lead to an increase in extracellular space (88). It is possible that when assessing viability, this injury can lead to increased T1 signal or R1 relaxation rate in areas of reversibly damaged myocardium because more contrast agent may enter the interstitium. Therefore, an increased distribution volume of contrast agent may not necessarily be an indication of irreversible injury.

**T1-weighted imaging**

Another factor may be that T1-weighted imaging techniques are affected by blood flow. Perfusion to regions of irreversibly damaged myocardium may be depressed significantly during reperfusion (no-reflow phenomenon) (2). Lower flow can limit the accessibility of contrast agent to areas of occlusive infarction immediately following injection and lead to hypoenhancement relative to the reperfused regions of infarction. Because, T1-weighted imaging is affected by both distribution and flow, it is our belief that Gd-DTPA-enhanced T1-weighted imaging alone may not be sufficient to differentiate reversibly from irreversibly injured tissues.

**T2*-weighted imaging**

Other researchers have attempted to use T2*-weighted imaging to assess viability. T2* is sensitive to hematocrit and hemorrhage as well as the homogeneity of the local

magnetic environment. When contrast agent flows into the capillaries, a microscopically heterogeneous distribution creates discrete magnetic gradients at the boundaries of the capillaries (11, 89-91). These local gradients result in the rapid decrease of T2* signal intensities or R2* rates. As the contrast agent crosses the capillary walls and diffuses into the interstitial space, the distribution of contrast agent becomes more homogeneous, leading to a recovery of T2* signal intensity. With irreversible injury, cell membrane integrity is lost and contrast agent can diffuse into the intracellular spaces. This may result in magnetic gradients becoming much more uniform due to the ubiquitous distribution. T2* signal intensity may then show a rapid recovery to pre-contrast values after an initial decrease on the first pass of contrast agent. Unfortunately, while R2* relaxation rates may be related to the degree of membrane damage, R2* may also be affected by the regional concentration of contrast agent. Relatively shorter R2* rates or higher T2* signal intensities may be due to a more homogenous distribution or a lower concentration. A shorter R2* or higher T2* signal intensity may indicate cell membrane damage only when the regional concentration of contrast agent is equal to or higher in a damaged region compared to a normal region. Therefore, we believe that the use of T2*-weighted imaging alone is insufficient for assessing myocardial injury.

# 3. Materials and Methods

## *3.1. Experimental design:*

Our experiments were designed to test the hypothesis that we could improve MR-based tissue viability assessments by observing T1 and T2* signal intensity time courses following a bolus injection of contrast agent. By observing T1 and T2* properties in the heart simultaneously, we postulated that it would be possible to measure perfusion and the dispersion/diffusion of a small molecular weight contrast agent. This is because contrast-enhanced T1 and T2*-weighted images are affected by different parameters. T1 is affected by the regional concentration of contrast agent, which will depend on perfusion. T2*-weighted image contrast is subject to the uniformity in distribution of contrast agent, which is affected by the loss of membrane integrity and diffusion of contrast agent into the intracellular space.

To test this hypothesis an experiment was designed that can be broken down into two parts:

1) Test the ability of simultaneous monitoring of T1 and T2* signal intensity to assess myocardial viability, with histologically stained heart sections as a references.
2) Compare our T1-T2* results to other, established, techniques that use either T1 or T2* relaxation time calculations to assess myocardial viability.

**Part 1: Use of T1-T2*-weighted imaging to assess myocardial infarction**

Myocardial infarction was induced and triphenyl tetrazolium stain was used to identify the region damage. This was correlated to the observed regions of damage found in T1-T2* MR imaging. Statistical analysis was performed to observe significance and the ability of the T1-T2* technique to differentiate between infarct and normal tissue.

**Part 2: Comparison of T1 and T2*-weighted imaging with T1-T2* technique**

The second part of the experiments compared the ability of T1-T2* imaging to identify myocardial damage to delayed contrast-enhanced MR imaging techniques (12, 13). We tested the ability of T1-T2* imaging against T1 and T2* relaxation times as a way to identify tissue viability. This was done by infusing contrast agent into infarcted hearts and using MR imaging to obtain T1 and T2* relaxation time values. Using the reciprocal of T1 and T2* time (R1 and R2* relaxation rate) we used statistical methods to test the ability of R1 and R2* relaxation rate measure to differentiate between infarct and normal tissue.

**Choice of animal model**

Domestic pigs were selected as the subjects for these experiments. The large animal model is considered to compare very well to humans and maintains the clinical significance of these studies. To create an infarction we chose to use swine that had been subjected to *in situ* occlusion of the left anterior descending coronary artery (LAD) for 2 hours, with a 1-hour reperfusion period. This is a well-established model that consistently led to significant levels of myocardial damage. Following reperfusion, the hearts were

excised and connected to a perfusion apparatus in the Langendorff mode for *ex vivo* MR imaging.

In Langendorff-style perfusion, perfusate is provided via the aorta. The pressure gradient causes the aortic valve to close and blood is forced through the coronaries. Normally, blood does not enter the left ventricle in this manner, so it does not pump any blood. This of course means that there is no external work. While Langendorff-style perfusion is a non-working model, it was used in order to the control various experimental parameters including temperature, coronary flow, and ionic composition of the perfusate. In addition, the non-beating model was preferred because of a limitation with cardiac MR imaging. Temporal resolution was inadequate to obtain clearly defined images in the beating heart, due to slow image acquisition.

**Perfusion System**

The perfusion system was composed of 3 parts: a perfusion pump, an oxygenator, and perfusion lines. A Precision Blood Pump (Kobe) connected to a Capoix 308 hollow-fiber oxygenator (Terumo Corp, Tokyo Japan) was used with a 20 mm arterial blood filter (model D735, Dideco, Mirandola, Italy). All arterial lines were made from Tygon tubing (Cole-Parmer, Chicago IL). In addition a water bath and heat exchangers (Shiley) were used to control perfusate temperature.

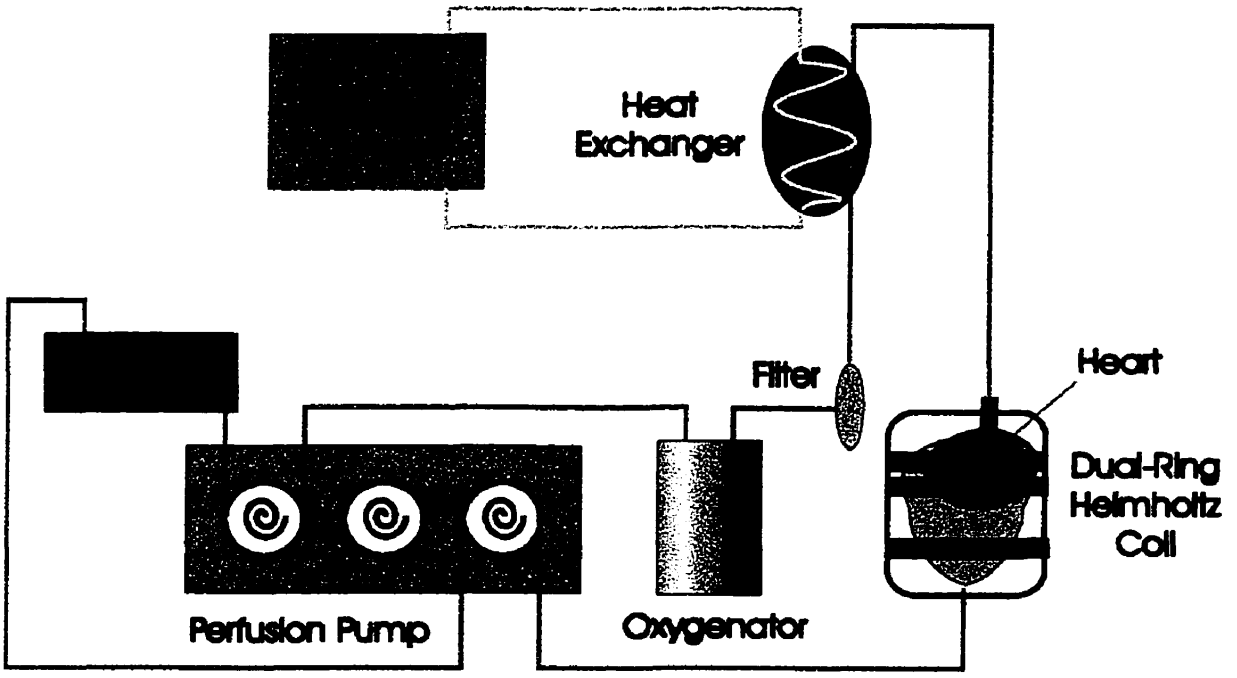


Figure 26. Setup and design of the experimental perfusion apparatus.

**Solutions and perfusates**

All solutions were prepared prior to experimentation using Ultrapure water and solutes obtained from the Sigma Aldrich Chemical Company. For heart perfusion a modified Krebs solution was prepared using:

| | | |
|---|---|---|
| NaCl – 102 mM | KCL – 16.79mM | $MgCl_2$ – 16 mM |
| EDTA – 0.5mM | Glucose – 11mM | $NaHCO_3$ – 25 mM |
| $CaCl_2$ – 1.28 mM | Bovine serum albumin – 0.625% | |

During occlusion of the coronary arteries, the heart was perfused with whole blood. However, following the LAD occlusion procedure, the pig was exsanguinated and a mixture of blood and Krebs solution was used to perfuse the excised heart in a

Langendorff manner. This mixture was monitored using a Statprofile 7+ blood gas analyzer (Nova Biomedical) to ensure blood pH was maintained at 7.4 ± 0.5. Hematocrit of this perfusate was measured at about 11-13%; magnesium and potassium were adjusted to 16 mM/L to prevent contraction of the heart.

**Notes**

We had intended to create a myocardial infarct as well as perform imaging *in vivo.* In fact, animals 1 and 2 were imaged *in vivo* with a specially designed surface coil. Unfortunately, the method proved to be technically difficult and no useable data were obtained from animals 1 and 2 following successfully surgery. Imaging with the *in vivo* surface coil was unacceptable due to poor homogeneity of the magnetic field.

For the remaining 8 animals the left anterior descending coronary artery was reversibly occluded to create a region of infarction. However, following *in vivo* reperfusion, the hearts were excised and perfused in Langendorff mode. This allowed imaging of the hearts *ex vivo* with a conventional, dual-ring, Helmholtz coil.

## 3.2 Surgical Preparation

The Animals used in this study received humane care in compliance with the Guide to the Care and Use of Experimental Animals formulated by Canadian Council on Animal Care. The National Research Council Animal Care Committee approved the protocols that are detailed in this study.

Ten domestic pigs (n = 10) weighing 20 – 25 kg were obtained and held in the animal facilities for two weeks prior to use. Surgery was successfully performed on the first two animals, but data were not collected due to technical difficulties with imaging the heart. The remaining eight hearts were prepared as follows.

Prior to experimentation, the pigs were fasted overnight and sedated with an intramuscular injection of diazepam (0.4 mg/kg) and ketamine (20 mg/kg). Anesthesia was maintained with 1-2 % isoflurane in a mixture of oxygen and nitrous oxide with respiratory rate and volume adjusted to keep arterial blood gases within the physiological range. Ventilation was monitored using an Excel 210 anesthesia system with a 5250 respiratory gas monitor (Ohmeda, Madison MI).

*In situ* coronary artery occlusion was performed by opening the chest via a midline sternotomy. Once the heart was exposed, the ascending aorta and the right atrial appendage were cannulated for emergent cardiopulmonary bypass whenever a lethal arrhythmia could not be converted to sinus rhythm (bypass was required in 5 out of 8 animals. Three animals required bypass immediately following occlusion, the remaining 2 animals required bypass 30 minutes following LAD occlusion). The femoral artery was cannulated to monitor arterial pressure. Blood gases were monitored using a Statprofile 7+ (NOVA Biochemical). A venous infusion line was established through an ear vein.

Pancuronium (0.2 mg/kg/1 - 2 hours) was administered through the venous infusion line as a muscle relaxant. Lidocaine was administered to reduce the incidence of ischemia-induced arrhythmia (initial bolus injection at 1 mg/kg followed by an intravenous instillation at 25 mg/kg/min thereafter).

To induce a massive myocardial infarction, the left anterior descending coronary artery (LAD) was occluded for 2 hours at its origin using a reversible surgical snare. The snare was then removed and the heart was allowed to reperfuse for 1 hour. The pig heart was then excised and mounted on a Langendorff perfusion apparatus. A mixture of autogenous blood and modified Krebs-Henseleit solution was used as perfusate for the heart (hematocrit was measured at 11-13 %). The concentrations of potassium and magnesium in the perfusate were each adjusted to 16 mmol/L to keep the heart quiescent throughout the imaging period. The heart was moved into the center of a 7 Tesla magnet and perfused at 50 - 60 mmHg. Throughout the *ex vivo* portion of the experiment, the pH and temperature of the perfusate were maintained at $7.4 \pm 0.5$ and $37^{0}$C, respectively. To prevent air-tissue interface artifacts in T2*-weighted images, the pig heart was immersed in the perfusate throughout the protocol.

## 3.3 Experimental Protocol

Once the *ex vivo* pig heart was placed inside the magnet, control (no contrast agent) T1 and T2* relaxation times were assessed using an inversion recovery technique. Gd-DTPA (0.05 mmol/kg) was then injected as a bolus through the perfusion line, entering the heart through the aorta. The dynamic T1 and T2* signal intensity changes

were monitored using an interleaved T1-T2* imaging sequence during the first pass of contrast agent.

After the concentration of the contrast agent in the perfusate reached a steady state level, which was ensured by observing a constant signal intensity in T1-weighted images over a 5 minute period, measurements of T1 and T2* relaxation times in the myocardium were repeated.

Following the MRI studies, the heart was removed from the magnet. Perfusion conditions were maintained and the heart was injected with colored microspheres to assess regional myocardial blood flow. Hearts were sectioned for TTC staining and microsphere analysis. TTC stained sections were used as references in analyzing the MR images and for selecting regions of interest as well as to identify regions to be analyzed for regional blood flow. The heart was sectioned according to a T1 scout image (long cardiac axis) to ensure a correlation to MR images.

## Magnetic Resonance Imaging

### 1) Hardware

Once the isolated heart was connected to the perfusion apparatus, it was placed in a dual-ring Helmholtz coil, designed to give a very uniform $B_1$ field throughout the sample volume and moved into a 7 Tesla, 40 cm horizontal bore Magnex MR scanner (Magnex Scientific) equipped with a Bruker console (Bruker Inc, Karlsruhe, Germany).

**2) Pulse Sequences**

Simultaneous monitoring of T1 and T2* signal intensities was performed using an interleaved T1-T2* imaging sequence (92, Figure 27). The sequence consists of one gaussian-shaped $90^0$ pulse (3.1 ms) followed by read and phase spoiler gradients to eliminate residual magnetization from the T2*-weighted imaging portion of the sequence. A 1.5 second delay was inserted to allow magnetization to relax back to equilibrium and then followed by a sech-shaped $180^0$ pulse (13 ms) to invert the magnetization, after which spoiler gradients were applied in all three directions. To acquire both T1 and T2* images in a single set of scans we used a dynamically variable echo time set to 4.2 ms for T1 and 15 ms for T2*-weighted imaging with repetition times of 6.75 and 18.15 ms, respectively.

Briefly described, the inversion pulse was active only for the T1-weighted portion. Once 128 phase encoding steps had been completed for the T1-weighted portion, there was a 1.2 ms delay followed by the T2*-weighted portion. Originally, the pulse sequence contained phase encoding rewinders, however these were removed and centric phase encoding was used to increase the temporal resolution, with little image degradation. The preparation portion of the sequence consisting of the $90^0$ pulse and spoiler gradients lasted 1524 ms. Each T1-weighted image was acquired in approximately 864 ms with T2*-weighted images acquired in 2324 ms. This sequence was repeated 50 times for a total of 100 images over 235 seconds.

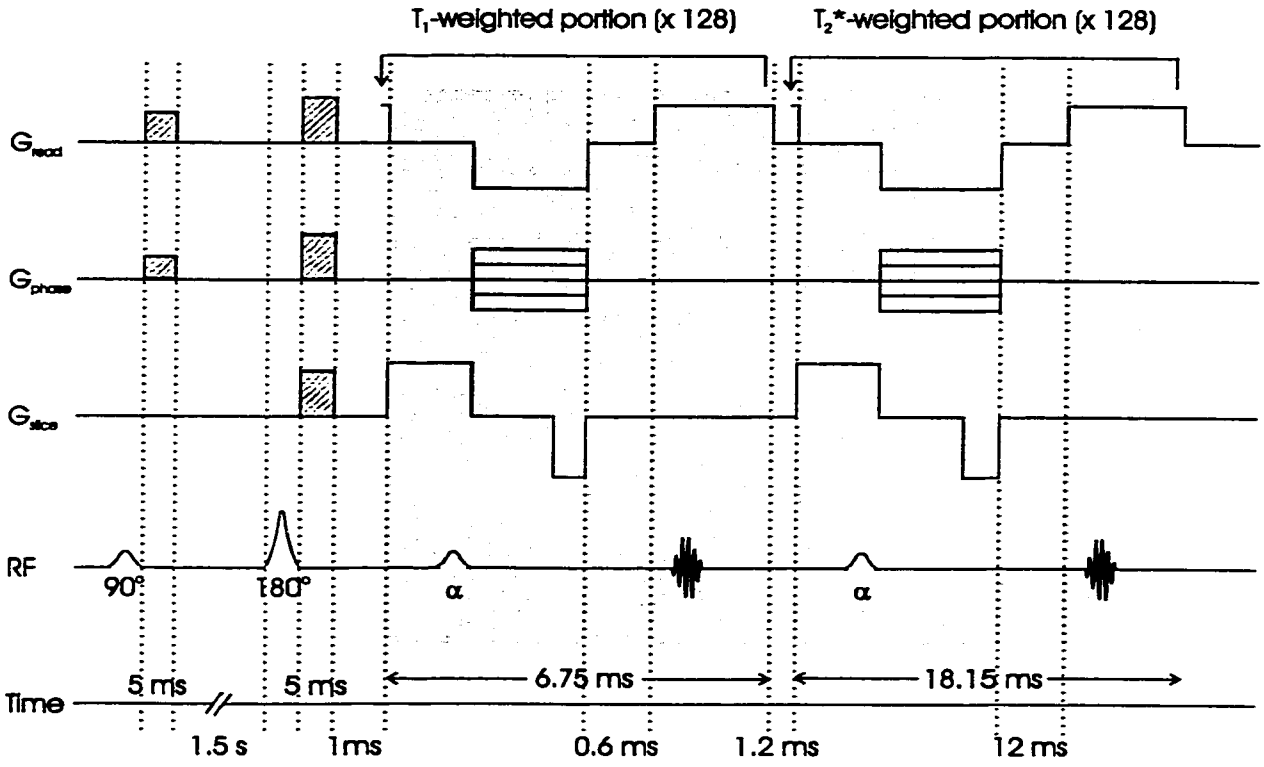


Figure 27. T1-T2* pulse sequence diagram

To compare this T1-T2* technique to contrast-enhanced relaxation rate techniques, we separately measured both R1 and R2*, the inverse of T1 and T2*. To measure T1 relaxation times, 14 images were acquired using a TurboFLASH sequence with 14 inversion recovery intervals (10, 50, 100, 200, 400, 800, 1000, 1400, 1800, 2200, 3000, 4000, 6000, and 10000 ms) in a total of 152 seconds. The signal intensities of these images were then fitted using the following function in the Marevisi software package (NRC – Institute for Biodiagnostics, Winnipeg. & Bruker Inc, Karlsruhe, Germany):

$$SI = A[1 - 2\exp(-(t-q)/\mathrm{T1})] \qquad (2)$$

where SI is signal intensity, A is initial signal intensity (at time zero), $t$ is the inversion recovery interval, and $q$ is the time shift between the calculated T1 (inversion recovery) and preset T1.

To measure T2* relaxation time, 4 MR images were acquired using a FLASH sequence with different echo times (4.6, 12, 20, and 25 ms) over 256 seconds. T2* relaxation times were then calculated in Marevisi by fitting image intensities with the function:

$$SI = A[\exp(-t/\mathrm{T2}^*)] \tag{3}$$

where $t$ is echo time, SI is signal intensity, and A is signal intensity at time zero.

All imaging (T1-T2*, T1, T2*) was performed with a slice thickness of 3 mm, field of view set at 12 x 12 cm, with a matrix size of 128 x 128 pixels. To minimize imaging time, only one slice was observed for each heart. However, to ensure that the level contained a sizable infarct several levels were observed prior to contrast agent injection.

## Colored Microsphere and TTC Staining Procedure

At the end of each experiment, approximately 5 x $10^6$ to 8 x $10^6$ non-radioactive red colored microspheres (15 ± 1.9 μm diameter, suspended in 2 ml of saline solution) were injected through the aorta via the perfusion line to measure regional myocardial blood flow. Arterial reference samples were withdrawn simultaneously from the ascending aorta at a constant rate of 5 ml/min for five minutes, starting one minute before the injection of microspheres. The heart was then removed from the perfusion system and sectioned. Alternating sections were used for triphenyl tetrazolium chloride staining with

the opposing side used for analysis of the colored microspheres. A proper spatial correlation to MR images was ensured by using a T1-weighted, long axis, scout image as a reference. Sections used for microsphere analysis were divided into 6 pie-shaped regions and tissue was collected from the endocardium, mid-myocardium, and epicardium. These sample regions were correlated to TTC-stained regions in the matched, opposing sections. The average weight of each sample was approximately 0.5 g.

Following collection, the tissue and blood samples were digested. The numbers of microspheres in the samples were counted using a spectrophotometer at a wavelength of 536 nm. Actual blood flow was obtained based on calculation of the microsphere count in the tissue and blood samples and the speed of blood collection.

## Data Analysis

Image data were processed using Marevisi and EvIdent 5.2 (NRC - Institute for Biodiagnostics, Winnipeg, Canada). Marevisi was used to determine the T1 and T2* relaxation times with the fitting functions described previously. Round, hand-drawn regions of interest (ROIs) were created by correlating the MR images to the TTC stained references. The size of the regions selected varied between hearts due to the variability in both heart size and size of infarction. However, the regions selected were approximately 400 pixels for normal, 300 pixels for reperfused, and 200 pixels for low-reflow infarct ROIs, while the total heart covered approximately 3500 pixels.

Statistical analyses were performed using Statistica (Statsoft Inc, Tulsa, Oklahoma, USA). One-way analysis of variance (ANOVA) with a Tukey's Honest Significant Difference test was used to compare R1 and R2* relaxation rates, percentage

recovery of T2* at maximum T1 signal intensity, and regional blood flow between normal, reperfused infarcted, and low-flow infarcted myocardium. A significant difference was said to exist at a probability value of less than 0.05. All numerical results are expressed as the mean ± standard error.

# 4. Results

## *4.1 TTC Staining and Regional Blood Flow*

A representative heart section (TTC-stained, short axis) is shown in Figure 28.

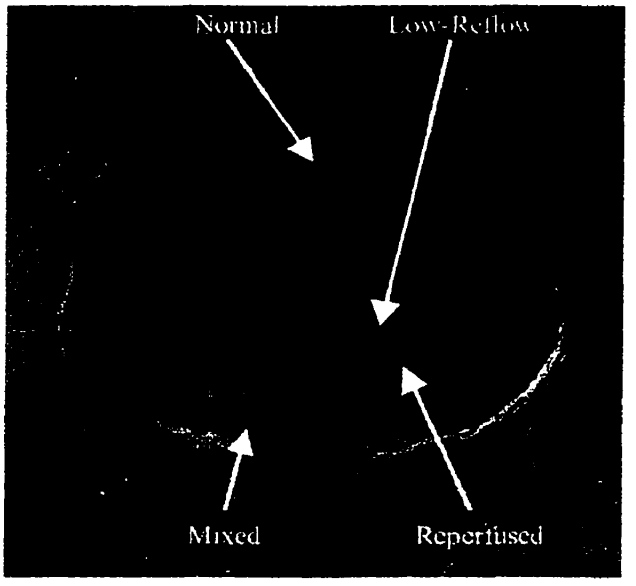


Figure 28. TTC-stained heart section showing tissue regions commonly observed during the experiments.
Note the red stained normal region, the pale reperfused infarct, and the pink non-reperfused infarct.

It is clear from the TTC staining that there is a large degree of heterogeneity in myocardial injury induced by 2-hours of occlusion of the LAD. Other than normally staining viable tissue, we observed regions of the myocardium that remained completely unstained (mid-myocardium in the LAD region), which suggests myocardial infarction. In addition, a core region in the infarction was lightly stained (subendocardium in the

LAD region) in all heart preparations. Several hearts also showed regions in the subepicardium that contained stained and unstained tissue, indicating the co-existence of viable and non-viable myocardium or a mixed region (4 out of 8 hearts).

Relating the TTC staining to blood flow measurements obtained from colored microsphere analysis (Figure 29), we found that the lightly stained region recorded the least amount of myocardial perfusion (0.123 ± 0.19 ml/g/min). This flow was significantly lower ($p < 0.05$) than in the normal (4.55 ± 0.48 ml/g/min) and unstained regions (1.20 ± 0.29 ml/g/min).

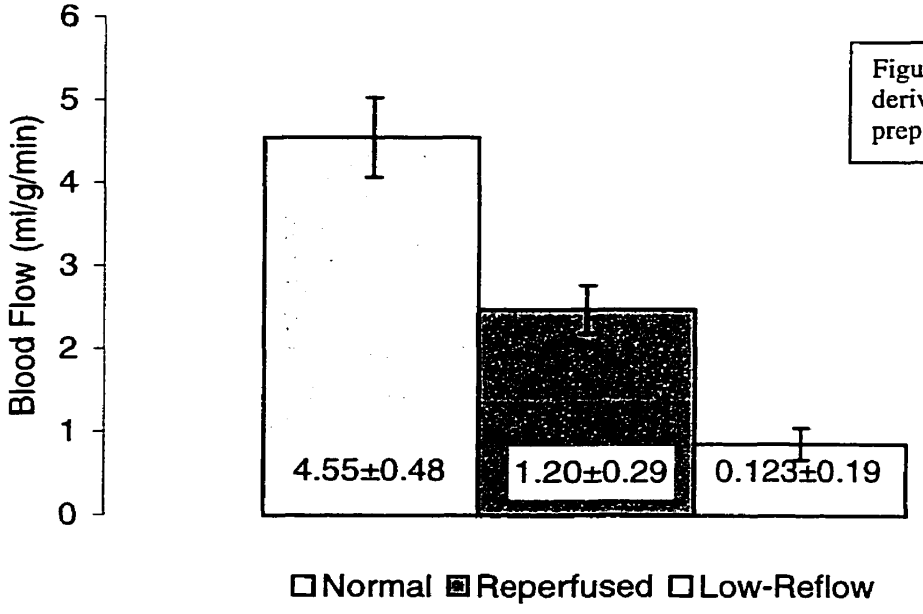


Figure 29. Blood flow data derived from 8 experimental preparations.

Histological sections of the pig hearts displayed severe blood cell sludging and trapping of colored microspheres in the capillaries of the lightly stained myocardium (Figure 30).

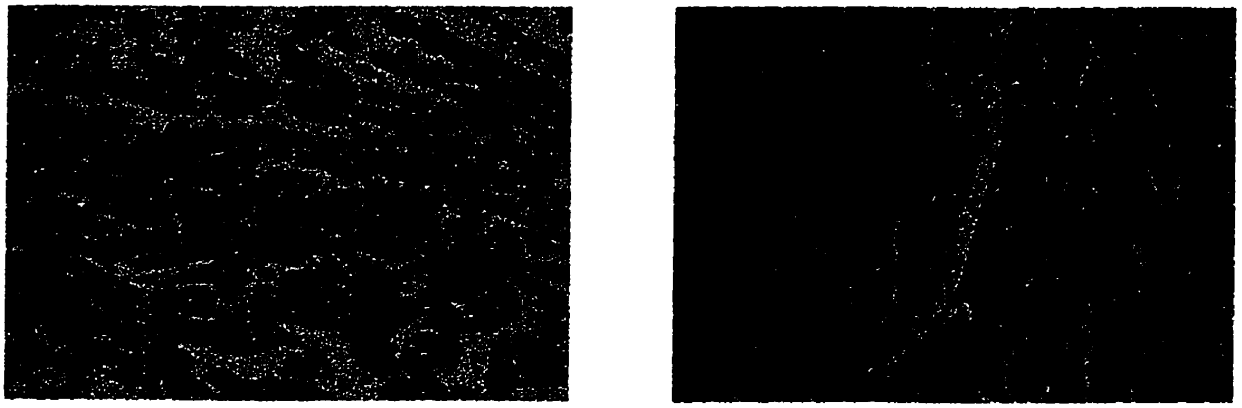

Figure 30. Microscopic analysis shows many trapped microspheres (indicated by arrows) in the low-reflow region of infarct (A) compared to the reperfused region (B).

These flow data and microscopic observations appear to indicate the existence of an occlusive infarction in the myocardium that showed light TTC staining. As a consequence, lightly stained and unstained tissues are referred to as low-reflow infarcted and reperfused infarcted myocardium, respectively. The non-LAD region, which stained brick red, is termed normal myocardium. The size and relative location of the reperfused, low-reflow, and mixed regions varied significantly between sections; but not all hearts in this study displayed a mixed region. Therefore blood flow and MRI parameters for this area were not analyzed.

## *Experiment 1: Percentage recovery of T2* signal at maximum T1*

Representative signal intensity time courses and MR images from one set of interleaved T1-T2* data are shown in Figures 31 and 32. The three regions of the myocardium exhibited very distinct temporal relationships between T1 and T2*. From Figure 31, it is apparent that there is a difference in the T2* recovery among regions of

myocardium. By evaluating this recovery at a set point, when T1 signal intensity reached its maximum level, we found significantly different values of T2* signal intensity recovery in the three regions (Figure 32). Low-reflow infarcted myocardium exhibited the greatest percentage recovery of T2* signal (90 ± 2.8 % of its initial value), followed by reperfused infarcted myocardium (63 ± 7.2 %). Normal myocardium displayed the least recovery of T2* signal intensity at maximum T1 signal (30.5 ± 2.4 %).

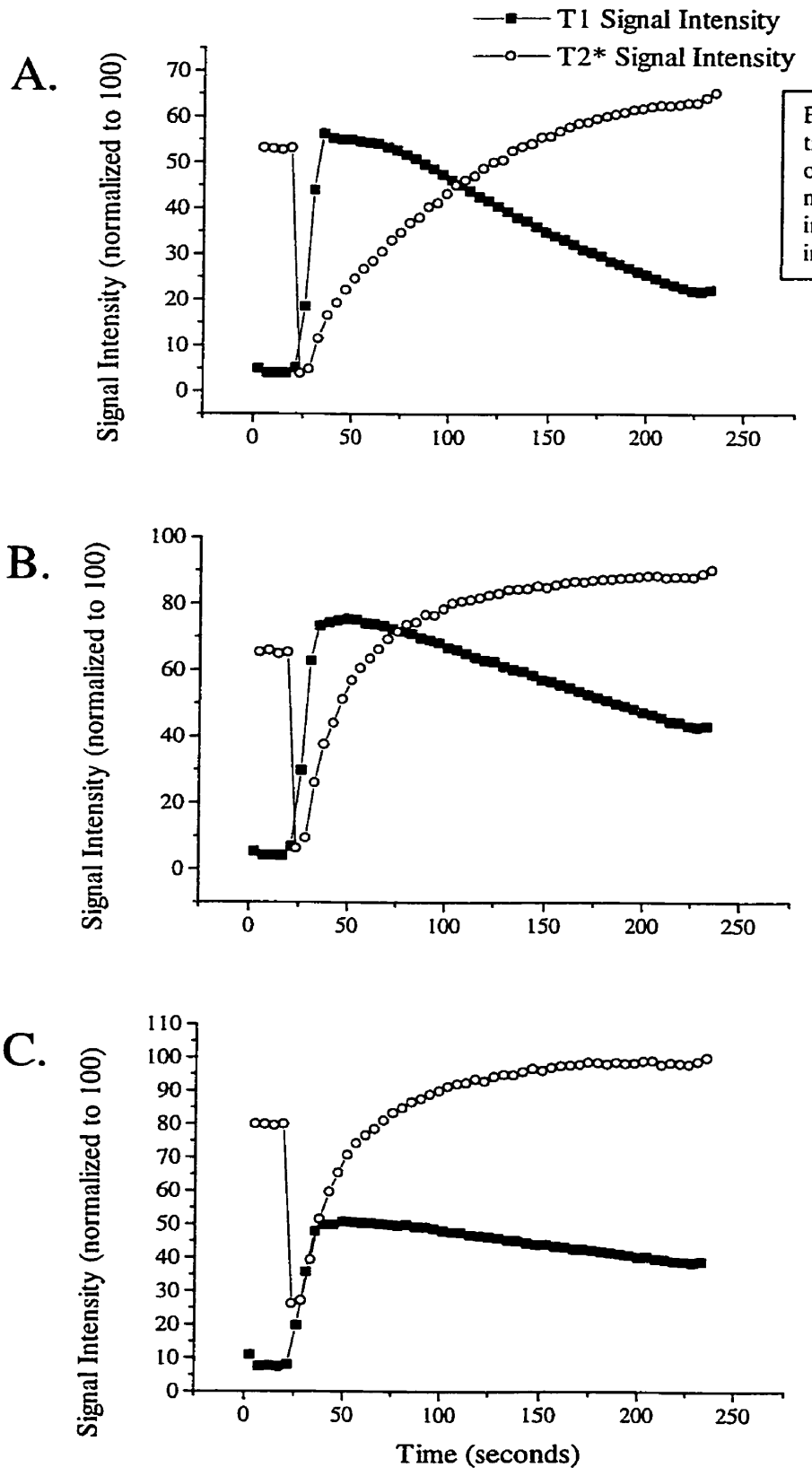


Figure 31. Sample T1-T2* timecourse data derives from one animal. A. Normal myocardium. B. Reperfused infarct. C. Low-reflow infarct.

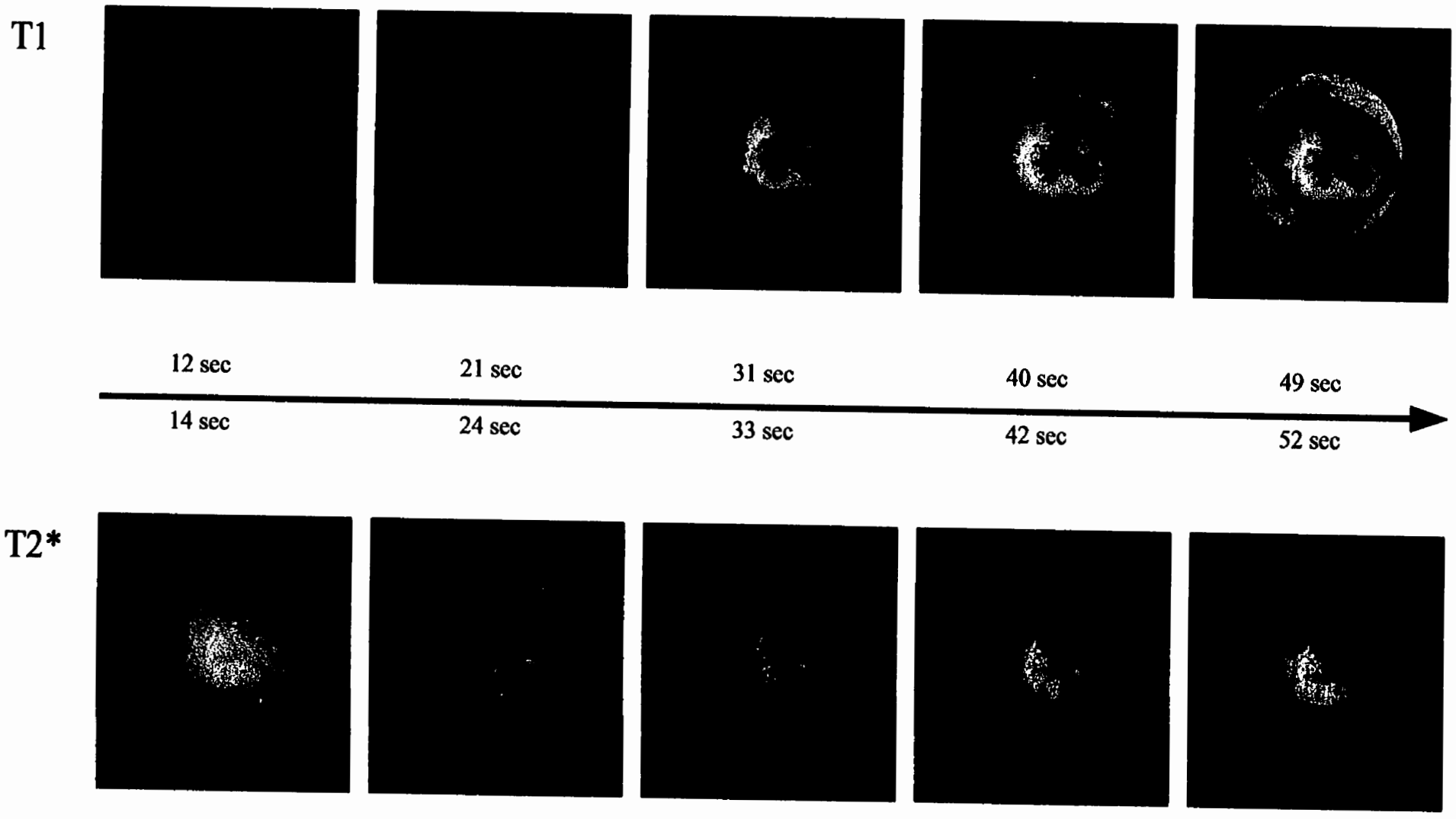


Figure 32. Representative $T_1$-$T_2$* images obtained during the first passage of Gd-DTPA. When observed at maximal $T_1$ signal intensity, more severely damaged myocardium (circled in red) exhibited greater recovery of $T_2$* signal intensity relative to normal myocardium. The recovery in normal tissue (circled in green) was delayed compared to the damaged regions

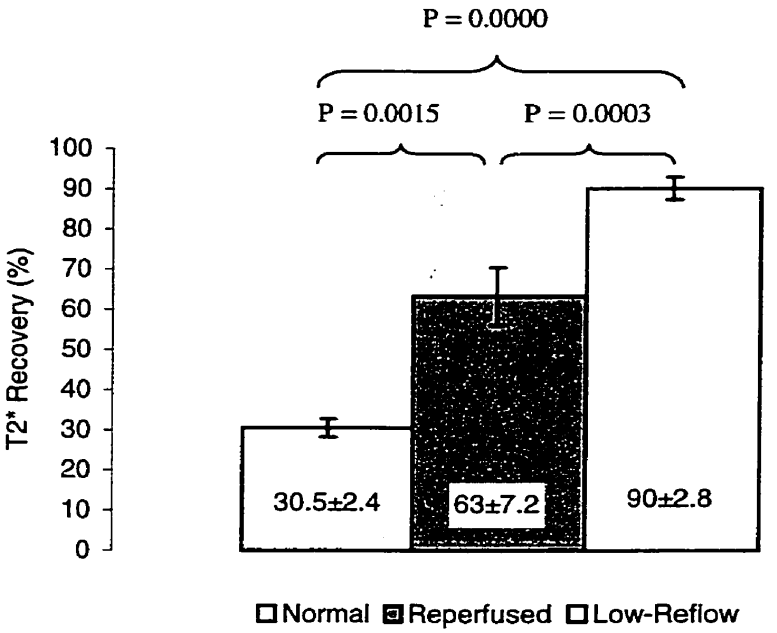


Figure 33. Summary of T2* recovery percentage averaged over all 8 preparations ± S.E.

**Clustering of data**

Noting the difference between signal intensity time course plots of our regions of interest, we used software to automate the identification. Using EvIdent 5.2 fuzzy clustering software we were able to identify groups of pixels that displayed similarity in their T1-T2* signal intensity time course data. This method was able to select regions in the MR data that showed similarity and resulted in an excellent correlation with TTC-stained sections. Several heart section images and regions identified by T1-T2* data clustering are shown in Figure 34. Each color in Figure 34 represents pixels that fall within the same cluster, or follow the same time course.

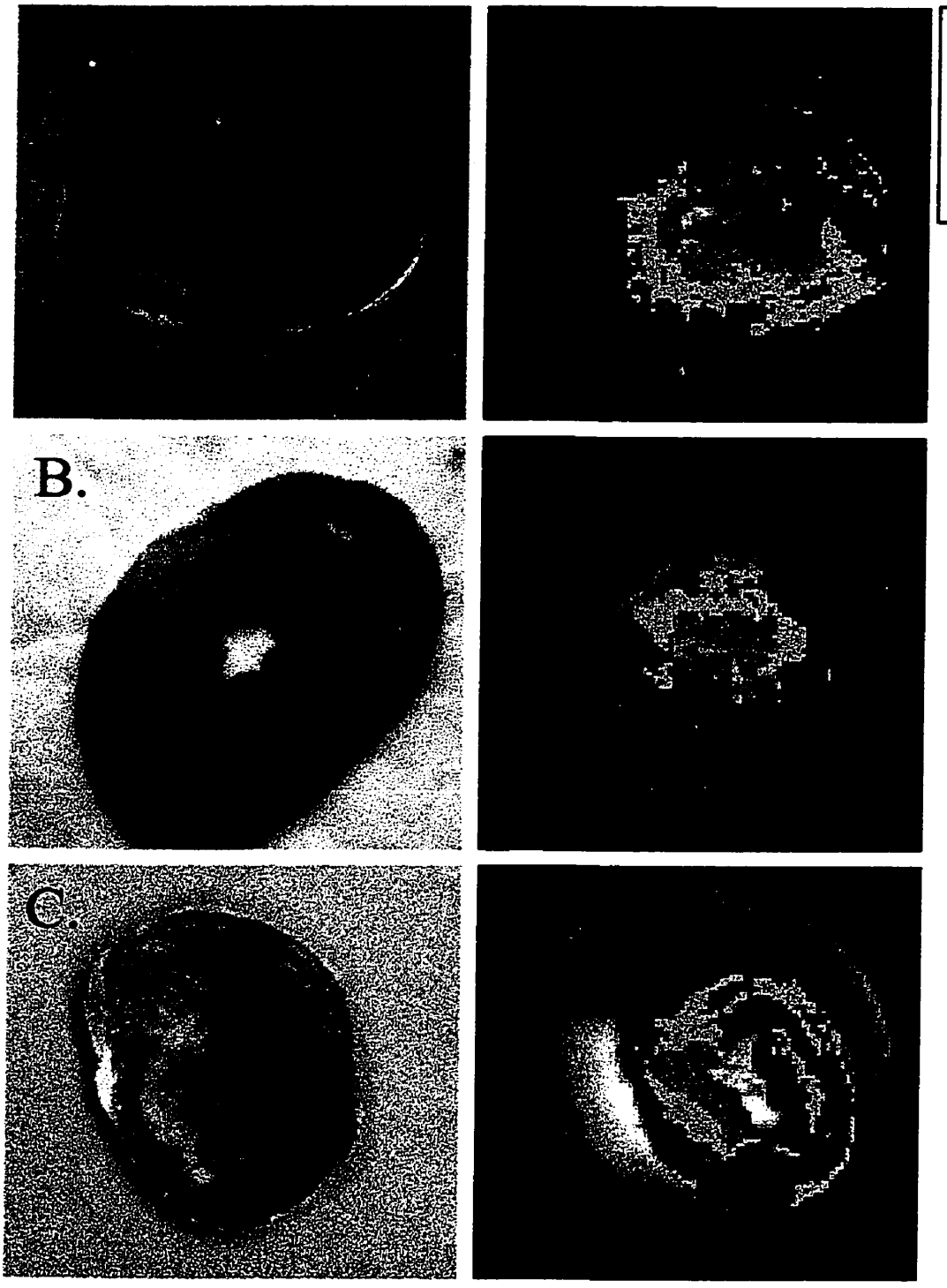


Figure 34. TTC-stained tissue and fuzzy cluster analysis of T1-T2* data shows a good match.

## *Experiment 2: R1 and R2* Relaxation Rate*

Sample post-contrast T1 and T2* maps are presented in Figure 35.

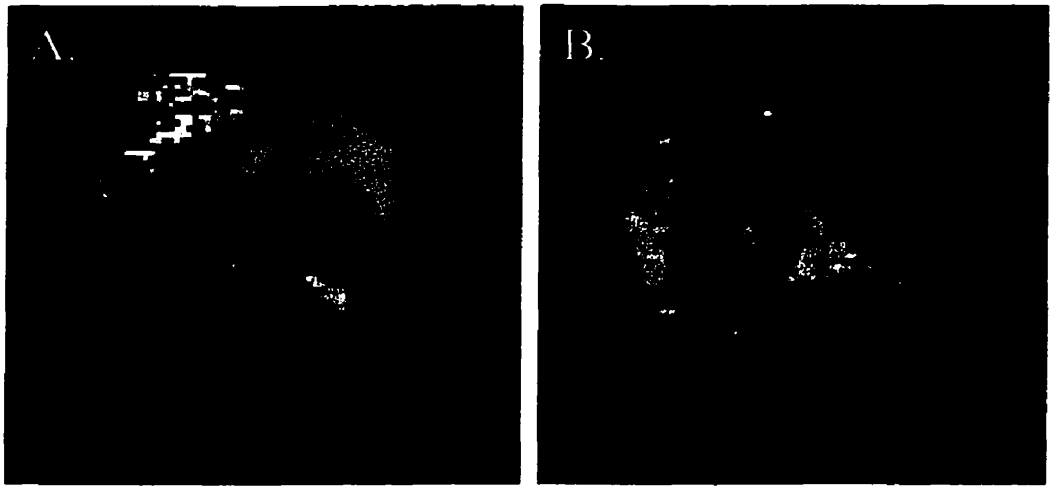


Figure 35. T1 and T2* relaxation time maps. A. T1 relaxation time. B. T2* relaxation time.

Average R1 relaxation rates measured with and without Gd-DTPA are shown in Figure 36. Prior to injection of Gd-DTPA (Figure 36a), R1 rates were significantly shorter in the reperfused infarcted and low-reflow infarcted myocardium relative to the normal region. Mean R1 values were $5.57 \pm 0.10 \times 10^{-4}$ $ms^{-1}$, $4.91 \pm 0.17 \times 10^{-4}$ $ms^{-1}$, and $4.37 \pm 0.16 \times 10^{-4}$ $ms^{-1}$ for normal, reperfused, and low-reflow infarct myocardium respectively. R1 relaxation rates measured with Gd-DTPA (Figure 36b) were significantly shorter in the low-reflow infarcted myocardium ($11.8 \pm 2.1 \times 10^{-4}$ $ms^{-1}$) than in the reperfused infarcted ($21.2 \pm 2.1 \times 10^{-4}$ $ms^{-1}$) and normal myocardium ($17.0 \pm 1.6 \times 10^{-4}$ $ms^{-1}$). The reperfused and normal myocardium exhibited similar R1 relaxation times in the presence of Gd-DTPA. However, Gd-DTPA-induced R1 shortening (ΔR1, Figure 36c) was significantly greater in the reperfused infarcted ($16.3 \pm 2.1 \times 10^{-4}$ $ms^{-1}$) than in

the low-reflow infarcted ($7.38 \pm 2.0 \times 10^{-4}$ $ms^{-1}$) and normal myocardium ($11.4 \pm 1.6 \times 10^{-4}$ $ms^{-1}$).

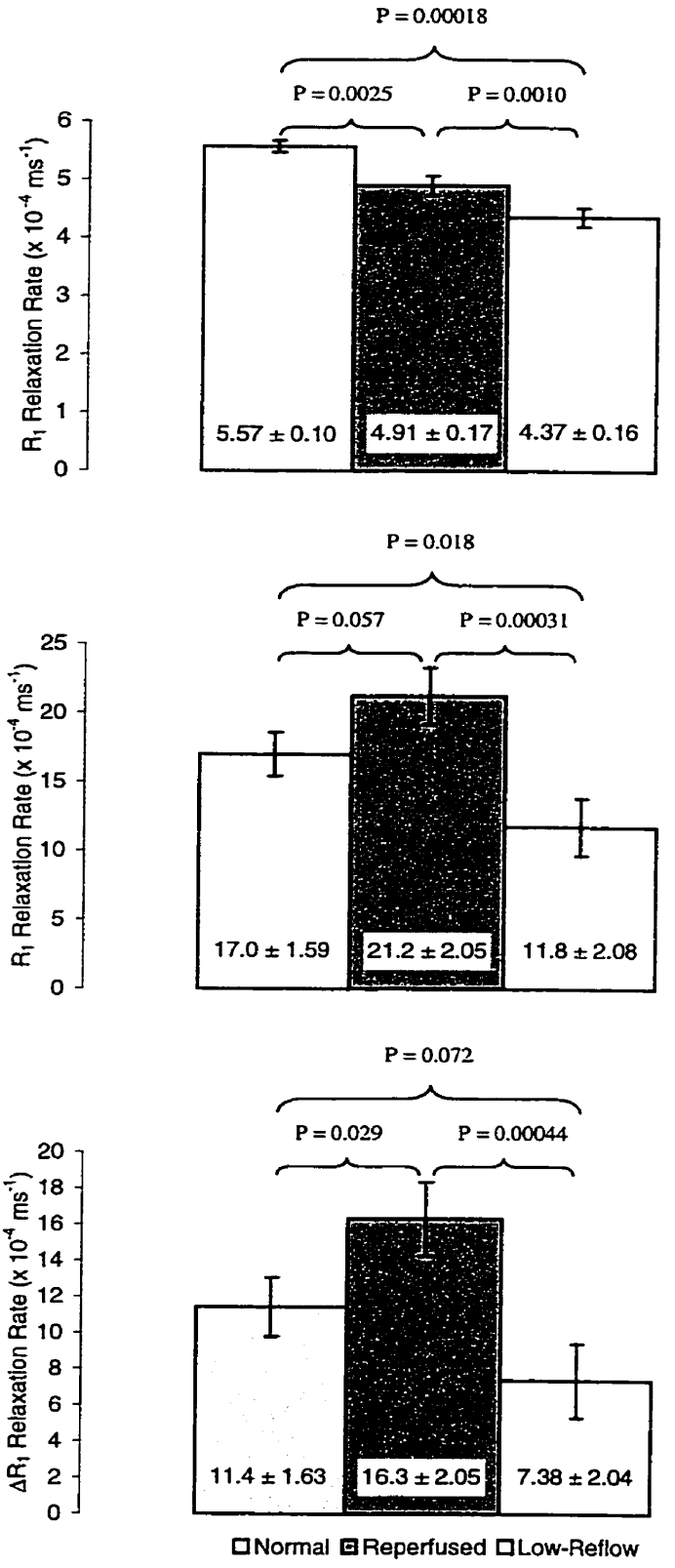


Figure 36. R1 relaxation rate data averaged over 8 preparations ± S.E.
A. Pre-contrast R1 rates
B. Post-contrast R1 rates
C. ΔR1 rates

Average R2* relaxation times measured without Gd-DTPA from normal, reperfused infarcted, and low-reflow infarcted myocardium were $3.62 \pm 0.23 \times 10^{-2}$ $ms^{-1}$, $2.60 \pm 0.18 \times 10^{-2}$ $ms^{-1}$, and $3.09 \pm 0.38 \times 10^{-2}$ $ms^{-1}$, respectively (Figure 37a). Normal and low-reflow infarcted myocardium showed similar R2* although their viability differed significantly. Following injection of contrast agent, both reperfused infarcted ($4.06 \pm 0.25 \times 10^{-2}$ $ms^{-1}$) and low-reflow infarcted myocardium ($4.36 \pm 0.37 \times 10^{-2}$ $ms^{-1}$) displayed a significantly shorter R2* relative to normal myocardium ($7.23 \pm 0.73 \times 10^{-2}$ $ms^{-1}$), as shown in Figure 37b.

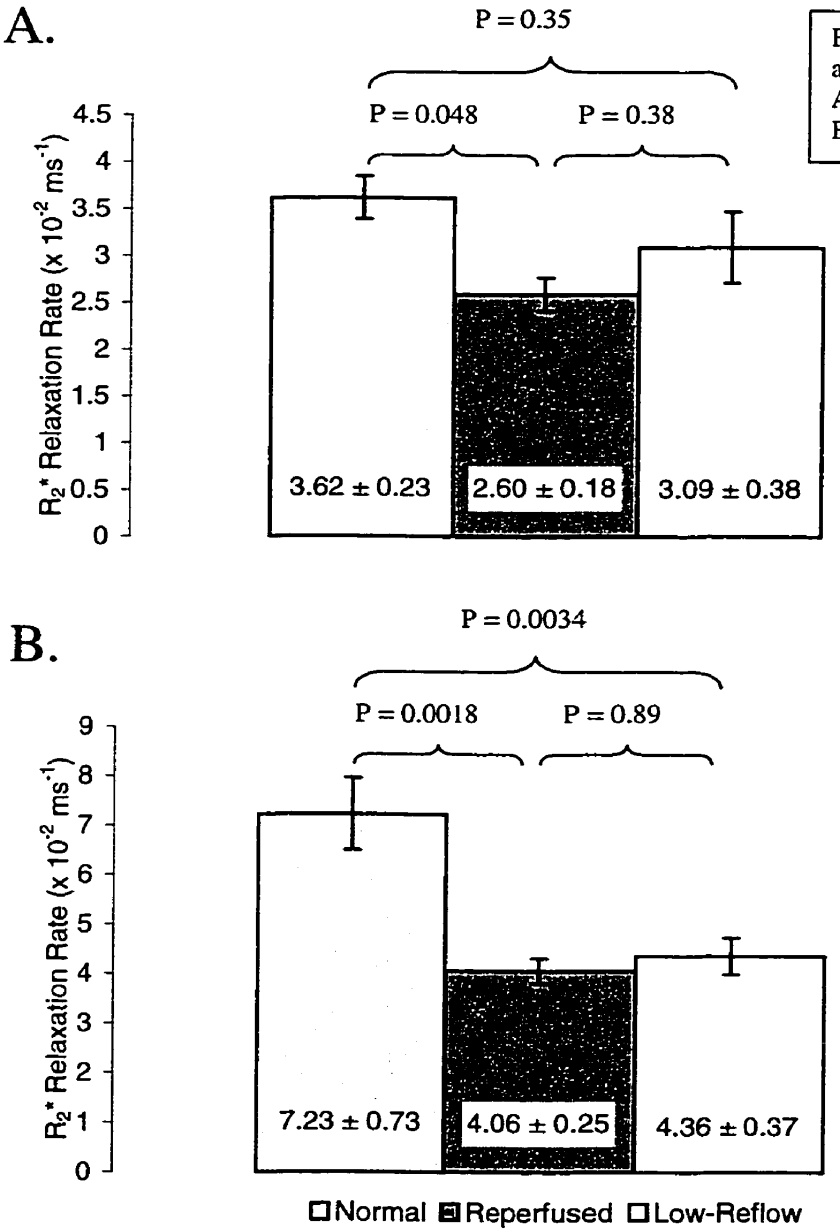


Figure 37. R2* relaxation rate data averaged over 8 preparations ± S.E.
A. Pre-contrast R2* rates
B. Post-contrast R2* rates

# 5. Discussion

The injury resulting from occlusion of a coronary artery results in very heterogeneous myocardial perfusion. This parameter can affect the analysis of MR image data. When studying contrast-enhanced T1-weighted images, perfusion of the contrast agent and redistribution leads to changes in signal intensity. When using T1-weighted imaging to assess myocardial viability, one needs to assume equal perfusion of the contrast agent in all regions of the heart. If so, irreversibly injured tissue will uniformly accumulate contrast agent in the intracellular compartment and lead to hyperenhancement on MR imaging. However typically there are regions of occlusive infarction, which on T1-weighted, contrast-enhanced imaging appear as regions of hypoenhancement compared to the reperfused (and hyperenhanced) infarct (89, 90, 93-95). One technique that has been used to circumvent perfusion differences is to use a continuous infusion of contrast agent, which allows redistribution and equilibration of the contrast agent in the extracellular space (13, 14, 79). Higher signal intensities observed in MR imaging are then assumed to result from higher intracellular concentrations of contrast agent, which are a consequence of passage through damaged cell membranes. Unfortunately, this required additional patient preparation time and exposure to contrast agents (13, 14, 79).

We have correlated regions of poor blood flow to TTC staining following a short reperfusion period. In normal myocardium, the presence of NADH (the reduced form of nicotinamide adenine dinucleotide) leads to the reduction of TTC dye to a brick red precipitate. In non-viable myocardium, which does not retain NADH, TTC is not reduced and the infarcted myocardium appears as a pale area on TTC stained sections. In addition,

we have observed lightly stained regions in the subendocardium in all heart preparations. This staining is likely due to incomplete washout of NADH resulting from extremely low regional blood flow following reperfusion. These findings were corroborated by analysis of colored microsphere distribution. Blood cell sludge in the capillaries, as observed in tissue sections, appears to be the major reason for the decrease in blood flow. The lightly stained region was used as an indication of occlusive or low-reflow infarction.

With interleaved T1-T2* imaging, there are distinct temporal relationships of T1 and T2* signal intensities during the first pass of Gd-DTPA (Figures 30 and 31). Normal myocardium shows a rapid decline to a minimal level of T2* signal intensity. This decrease in T2* signal intensity may be due to a heterogeneous distribution of contrast agent as it passes through the capillaries and is confined to intravascular spaces. Corresponding T1 signal intensity is relatively low, presumably due to confinement of the contrast agent to the intravascular space, a compartment that accounts for a small percentage (approximately 5%) of total tissue volume. As contrast diffuses into the interstitial space, T1 signal intensity reaches its peak level. Infiltration of Gd-DTPA into tissue may decrease micro-gradients across the capillary walls, leading to recovery of T2* signal intensity. Because Gd-DTPA cannot diffuse into the intracellular space in normal myocardium, the distribution of contrast agent remains relatively heterogeneous. Consequently, T2* signal intensity displays a small percentage recovery when the concentration of contrast agent reaches its maximal level (manifested by peak T1 signal). Further recovery of T2* signal intensity in the normal myocardium is mostly related to washout of the contrast agent.

In the reperfused infarct region, Gd-DTPA may not only diffuse into the interstitial space, but also into the intracellular space. The distribution of contrast agent becomes more homogeneous relative to that in normal myocardium when the regional concentration of contrast agent reaches its maximum level, which leads to a greater percentage recovery of T2* signal intensity at maximum T1 signal intensity than in normal myocardium.

The low-reflow infarcted zone displays low levels of reperfusion. As a result, the amount of contrast agent delivered to the region is limited, leading to a smaller increase in T1 signal intensity during the first pass of Gd-DTPA relative to that observed in reperfused infarcted myocardium. Although the total concentration of contrast agent is significantly less than in the reperfused infarcted region, the relative distribution volume in the low-reflow infarcted region supported by the intact capillaries may be larger in the low-reflow than in the reperfused infarcted regions. This may explain the higher percentage recovery of T2* signal intensity. It may also suggest more severe damage to cell membrane integrity in the low-reflow region relative to that in reperfused infarcted myocardium. Therefore, we believe that the percentage recovery of T2* during the first pass of Gd-DTPA may be related to the degree of myocardial injury.

Lastly, we note the distinct shapes of the time courses in tissues with differing viability and perfusion. Using the EvIdent clustering package on our T1-T2* data, we were able to identify regions of interest that closely matched the TTC stained sections. Using the clustering feature of the software, it was possible to automatically pick out regions in the MR images that showed similar changes in signal intensity.

Using TTC-based tissue classification, we found that prior to injection of contrast agent the R1 relaxation rates in the infarcted regions of the myocardium (low-reflow and reperfused) were indistinguishable. Each showed a similar R1 value (Figure 36a). This likely resulted from the accumulation of water or interstitial fluid in infarcted tissues. Administration of contrast agent shortened these relaxation times to differing degrees. R1 increased to a greater degree in the reperfused infarcted areas than in normal or low-reflow stained areas of the myocardium, implying a greater amount of contrast agent accumulated in the region. Our interpretation is that damage to cell membranes in the reperfused infarcted myocardium allowed contrast agent to penetrate the intracellular spaces leading to an increase in effective distribution volume of the contrast agent (10-12). The low-reflow infarct did not show an R1 increase similar to that observed in the reperfused region of infarction. This was most likely due to poor flow. Based solely on R1, our results would lead to an inaccurate assessment of tissue viability. Observation of R1 early after contrast injection cannot completely differentiate between damaged and normal myocardium.

As with R1, R2* relaxation rates may be influenced a number of factors. With R2* both the concentration and heterogeneity of distribution of contrast agent can alter the relaxation rate. Initially R2* was shorter in the reperfused infarcted myocardium, indicating homogeneity in the local magnetic environment. However, low-reflow infarcted tissue showed a surprisingly long R2* relaxation rate. This may be related to intra-myocardial hemorrhage that was observed in the region (blood cell sludging). Red blood cells and deoxymyoglobin trapped in the tissue can result in magnetic susceptibility effects that lengthen R2* rate (12). Following injection of contrast agent, the reperfused

myocardium displayed significantly shorter R2* relative to normal tissue. The R2* rate remained highest in reperfused infarcted myocardium, which may be the result of loss of membrane integrity. The R2* rate in the low-reflow region was not significantly different from that in normal or reperfused infarcted myocardium, which may be related to attenuated blood flow in the former.

## *Limitations and future work*

In this study, we did not assess the distribution volume or the homogeneity of distribution of Gd-DTPA directly. At present, it is still a working hypothesis that the percentage recovery of T2* signal intensity depends on the severity of membrane injury, which remains to be determined. In addition, a field strength of 7 Tesla was used, which had the effect of decreasing imaging time and increasing the T2* effect. Future applications of the T1-T2* technique will need to deal with lower levels of T2* contrast, which will result from use of clinical MR scanners that operate at lower magnetic fields that the one used in this study. One way of overcoming this limitation would be to use contrast agents that preferentially affect T2/T2* relaxation, or magnetic susceptibility agents such as dysprosium-DTPA. Furthermore, our experiments were conducted on a non-beating, ex vivo heart model. Clinical work may be complicated by cardiac contraction and significantly different blood flow patterns than that which was observed. It is important that image acquisition time be reduced to allow imaging of beating hearts. This may be accomplished by using echo-planar imaging, however these types of imaging sequences trade image detail for imaging time. The trade-off will need to be explored in future applications. One last concern may be the blood flow rates that were

observed in our acute model. In a clinical situation, following a longer period of reperfusion, regions of the reperfused infarction may have a level of blood similar to that of normal myocardium. While it is not expected that this will have any adverse affect on the identification of nonviable tissue, variations in blood flow within the infarcted myocardium should be explored.

## Summary

The distribution of myocardial injury resulting from the occlusion of a coronary artery can be very heterogeneous. One aspect of the diversity was seen in the regional blood flow patterns measured with microsphers. These patterns may be important since dissimilar regional perfusion often indicates the presence of both reperfused and occlusive infarct zones. With contrast-enhanced MR, a perfusion mismatch affects the distribution of contrast agent and can be observed as hyper- and hypo-enhanced regions. It has been proposed that the observation of these zones may have clinical relevance, as the presence of an occlusive infarct (hypo-enhanced region on early contrast-enhanced imaging) may indicate poorer late functional recovery (83, 84). However, relying on a single measurement of T1 or T2* signal intensity can lead to errors in identifying the extent of infarction, particularly when an occlusive infarct is juxtaposed to viable myocardium (as seen at the lateral boundaries of the lightly stained region in Figure 28, and its corresponding T1/T2* maps; 35a/b). Periera et al. (13, 14) have suggested that to improve the evaluation of infarction a continuous infusion of contrast media may be used with calculation of the partition coefficient. However, this method is limited by additional time and contrast agent requirements. Also, recent reports suggest that constant infusion

may overestimate the limits of infarction (16). Our technique improves on both previously mentioned procedures. Using a single bolus injection of contrast agent we are able to observe the hypo-enhanced region as well as differentiate normal and infarcted myocardium.

# References

1. Bolli R. Why myocardial stunning is clinically important. Basic Res Cardiol. 1998; 93: 169-172.

2. Kloner A, Bolli R, Marban E, Reinlib L, Braunwald E. Medical and cellular implications of stunning, hibernation, and preconditioning. Circulation. 1998; 97: 1848-1867.

3. Menasché P, Galiñanes M. Is myocardial stunning of clinical importance? A surgeon's perspective. Basic Res Cardiol. 1998; 93: 167-168.

4. Rahimtoola SH. From coronary artery disease to heart failure: Role of the hibernating myocardium. Am J Cardiol. 1995; 75: 16E-22E.

5. Ventura HO, Price HL, Smart FW, Stapleton DD, Van Meter CH. Cardiac transplantation in older patients: Changing perspectives. In: Messerli FH, ed. Cardiovascular disease in the elderly. 3rd edition. Dordrecht: Kluwer Academic Publishers, 1993: 555-562.

6. Fisch C. Echocardiography. In: Braunwald E. Heart Disease: A textbook of cardiovascular medicine. 4th edition. Pennsylvania: W.B. Saunders Company, 1992: 64-115.

7. Zaret BL, Wackers FJT, Soufer R. Nuclear Cardiology. In: Braunwald E. Heart Disease: A textbook of cardiovascular medicine. 4th edition. Pennsylvania: W.B. Saunders Company, 1992: 276-311.

8. Higgins CB. Newer cardiac imaging techniques (CT, MRI). In: Braunwald E. Heart Disease: A textbook of cardiovascular medicine. 4th edition. Pennsylvania: W.B. Saunders Company, 1992: 312-341

9. Saeed M, Wendland MF, Higgins CB. Contrast Media for MR Imaging of the Heart. J Magn Reson Imaging. 1994; 4: 269-279.

10. Saeed M, Bremerich J, Wendland MF, Wyttenbach R, Arheden H, Weinmann HJ, Higgins CB. MRI quantification of salvagable myocardium in ischemia/reflow injury by dynamic and quasi-equilibrium distribution of contrast media. Circulation. 1998; 98 (suppl): I-372.

11. Lima JAC, Judd RM, Bazille A, Schulman SP, Atalar E, Zerhouni EA. Regional heterogeneity of human myocardial infarcts demonstrated by contrast-enhanced MRI: Potential Mechanisms. Circulation. 1995; 92: 1117-1125.

12. Wu KC, Zerhouni EA, Judd RM, Lugo-Olivieri CH, Barouch LA, Schulman SP, Blumenthal RS, Lima JAC. Prognostic significance of microvascular obstruction by Magnetic Resonance Imaging in patients with acute myocardial infarction. Circulation. 1998; 97: 765-772.

13. Pereira RS, Prato FS, Sykes J, Wisenberg G. Assessment of myocardial viability using MRI during a constant infusion of Gd-DTPA: Further studies at early and late periods of reperfusion. Magn Reson Med. 1999; 42: 60-68.

14. Periera RS, Prato FS, Wisenberg G, Sykes J. The determination of myocardial viability using Gd-DTPA in a canine model of acute myocardial ischemia and reperfusion. Magn Reson Med. 1996; 36: 684-693.

15. Canadian Pharmacists' Association. CPS: Compendium of pharmaceuticals and specialties. 34th edition. Toronto: Webcom, 1999: 989-990.

16. Saeed M, Bremerich J, Wendland MF, Wyttenbach R, Weinmann HJ, Higgins CB. Reperfused myocardial infarction as seen with the use of necrosis-specific versus standard extracellular MR contrast media in rats. Radiology. 1999; 213(1): 247-57.

17. Opie LH. Fuels: Carbohydrates and lipids. In: Opie LH. The heart: Physiology and metabolism. 2nd edition. New York: Raven Press, 1991: 208-246.

18. Opie LH. Substrate and energy metabolism of the heart. In: Sperelakis N, ed. Physiology and pathophysiology of the heart. 3rd edition. Dordrecht: Kluwer Academic Publishers, 1995: 385-411.

19. Opie LH. Oxygen supply: coronary flow. In: Opie LH. The heart: Physiology and metabolism. 2nd edition. New York: Raven Press, 1991: 277-300.

20. Fleg JL, Gerstenblith G, Lakatta EG. Pathophysiology of the aging heart and circulation. In: Messerli FH, ed. Cardiovascular disease in the elderly. 3rd edition. Dordrecht: Kluwer Academic Publishers, 1993: 27-58.

21. De Jong JW, Achterberg PW. ATP-metabolism in normoxic and ischemic heart. In: De Jong JW, ed. Myocardial energy metabolism. Dordrecht: Martinus Nijhoff, 1988: 3-8.

22. Mayes PA. Glycolysis and the oxidation of pyruvate. In: Murray RK, Granner DK, Mayes PA, Rodwell VW, eds. Harper's Biochemistry. 24th edition. Connecticut: Appleton and Lange, 1996: 177-184.

23. Lehninger AL, Nelson DL, Cox MM. Principles of biochemistry.2nd edition. New York: Worth Publishers, 1993: 400-445.

24. Voet D, Voet JG. Biochemistry. 2nd edition. New York: John Wiley and Sons, 1995: 443-483.

25. Lehninger AL, Nelson DL, Cox MM. Principles of biochemistry.2nd edition. New York: Worth Publishers, 1993: 446-505.

26. Voet D, Voet JG. Biochemistry. 2nd edition. New York: John Wiley and Sons, 1995: 538-562.

27. Mayes PA. Biological oxidation. In: Murray RK, Granner DK, Mayes PA, Rodwell VW, eds. Harper's Biochemistry. 24th edition. Connecticut: Appleton and Lange, 1996: 116-122.

28. Mayes PA. Oxidation of fatty acids: Ketogenesis. In: Murray RK, Granner DK, Mayes PA, Rodwell VW, eds. Harper's Biochemistry. 24th edition. Connecticut: Appleton and Lange, 1996: 224-235.

29. Voet D, Voet JG. Biochemistry. 2nd edition. New York: John Wiley and Sons, 1995: 563-598.

30. Armstrong WF. Acute myocardial ischemia: from Tennant and Wiggers to contrast echocardiography. J Am Coll Cardiol. 1986; 2: 393-394.

31. Opie LH. Myocardial ischemia-metabolic pathways and implications of increased glycolysis. Cardiovasc Drugs Ther. 1990; 4[suppl 4]: 777-90.

32. Lawson JWR, Uyeda K. Effects of insulin and work on fructose 2,6-bisphosphate content and phosphofructokinase activity in perfused rat hearts. J Biol Chem. 1987; 262: 3165-3173.

33. Neely JR, Whitmer JT, Rovetto MJ. Inhibition of gylcolysis in hearts during ischemic perfusion. In: Harris P, Bing RJ, Fleckenstein A, eds. Recent Advances in studies on cardiac structure and metabolism. Maryland: University Park Press, 1976: 243-248.

34. Opie LH. Substrate utilization and glycolysis in the heart. Cardiology. 1971; 56: 2-21.

35. Sperelakis N. Basis of cardiac resting potential. In Sperelakis N, ed. Pathophysiology of the heart. Boston: Kluwer Academic Publishers, 1995: 55-76.

36. Kass RS. Ionic basis of electrical activity in the heart. In Sperelakis N, ed. Physiology and pathophysiology of the heart. Dordrecht: Kluwer Academic Publishers, 1995: 77-90.

37. Garratt KN, Morgan JP. Coronary circulation: Pathophysiology of myocardial ischemia and reperfusion. In: Giuliani ER, Fuster V, Gersh BJ, McGoon MD, McGoon DC, eds. Cardiology: Fundamentals and Practice. 2nd edition. St. Louis: Mosby Year Book, 1991: 1150-1158.

38. Patterson E, Scherlag BJ, Lazzara R. Cellular electrophysiology and ischemia. In Sperelakis N, ed. Pathophysiology of the heart. Boston: Kluwer Academic Publishers, 1995: 547-564.

39. Pasternak RC, Braunwald E, Sobel BE. Acute myocardial infarction. In: Braunwald E ed. Heart Disease: A textbook of cardiovascular medicine. 4th edition. Pennsylvania: W.B. Saunders Company, 1992: 1200-1291.

40. Braunwald E, Sobel BE. Coronary blood flow and ischemia. In. Braunwald E. Heart Disease: A textbook of cardiovascular medicine. 4th edition. Pennsylvania: W.B. Saunders Company, 1992: 1161-1199.

41. Opie LH. Cell death and myocardial infarction. In: Opie LH, ed. The heart: Physiology and metabolism. 2nd edition. New York: Raven Press, 1991: 451-468.

42. Reimer KA, Hill ML, Jennings RB. Prolonged depletion of ATP and of the adenine nucleotide pool due to delayed resynthesis of adenine nucleotides following reversible myocardial ischemic injury in dogs. J Mol Cell Cardiol. 1981; 13: 229.

43. Zabel M, Hohnloser SH, Koster W, Prinz M, Kasper W, Just H. Analysis of creatine kinase, CK-MB, myoglobin and troponin T time-activity curves for early assessment of coronary artery reperfusion after intravenous thrombolysis. Circulation. 1993; 87: 1542.

44. Adams JE, Abendschein DR, Jaffe AS. Biochemical markers of myocardial injury. Is MB creatine kinase the choice for the 1990's? Circulation. 1993; 88: 750.

45. Corr PB, McHowat J, Yan GX, Yamada KA. Lipid derived amphiphiles and their contribution to arrhythmogenesis during ischemia. In Sperelakis N, ed. Pathophysiology of the heart. Boston: Kluwer Academic Publishers, 1995: 527-546.

46. Fleckenstein-Grun G. Intracellular calcium overload – a cytotoxic principle: Cellular protection by calcium antagonists. In: Opie LH, ed. Myocardial protection by calcium antagonists. New York: Wiley-Liss, 1994: 29-45.

47. Bolli R. Causative role of oxyradicals in myocardial stunning: a proven hypothesis. Basic Res Cardiol. 1998:93:156-162

48. Opie LH. Myocardial reperfusion: Calcium and free radicals. In: Opie LH, ed. The heart: Physiology and Metabolism. 2nd edition. New York: Raven Press, 1991: 469-483.

49. Solaro RJ. Control mechanisms regulating contractile activity in the heart. In Sperelakis N, ed. Physiology and pathophysiology of the heart. Boston: Kluwer Academic Publishers, 1995: 355-366.

50. Dhalla N, Elimban V, Rupp H, Takeda N, Nagano M. Roles of calcium in cardiac cell damage and dysfunction. In Sperelakis N, ed. Physiology and pathophysiology of the heart. Boston: Kluwer Academic Publishers, 1995: 605-624.

51. Marban E. Pathogenic role for calcium in stunning? In: Lionel H. Opie, ed. Stunning Hibernation, and calcium in myocardial ischemia and reperfusion. Norwell, MA: Kluwer; 1992:83-87

52. Lie JT. Pathology of coronary artery disease. In: Giuliani ER, Fuster V, Gersh BJ, McGoon MD, McGoon DC, eds. Cardiology: Fundamentals and Practice. 2nd edition. St. Louis: Mosby Year Book, 1991: 1211-1231.

53. Braunwald, E. Stunning of the myocardium: an update. In: Lionel H. Opie, ed. Stunning, hibernation, and calcium in myocardial ischemia and reperfusion. Norwell, MA: Kluwer; 1992:4-9

54. Kaneko M, Matsumoto Y, Hayashi H, Kobayashi A, Yamazaki N. Oxygen free radicals and calcium homeostasis in the heart. Mol Cell Biochem. 1994; 139(1): 91-100.

55. Hearse DJ. Ischemia, reperfusion and the determinants of tissue injury. Cadiovasc Drugs Ther. 1990; 4: 767-776.

56. Buja LM, Modulation of myocardial response to ischemia. Lab Invest. 1998:78:11:1345-1373

57. Opie, LH. Myocardial reperfusion: new ischemic syndromes. In: Opie LH, ed. The Heart: Physiology and metabolism. 3rd edition. Philadelphia, PA: Lippencott-Raven; 1998:563-588

58. Opie, LH. Myocardial stunning - we do not know the mechanism nor is there "overwhelming evidence" for a major role of free radicals. Basic Research in Cardiology. 1998:93:152-155

59. Shattock MJ, Do we know the mechanism of stunning? Basic Research in Cardiology. 1998:145-149

60. Schulz R, Heusch G. Characterization of hibernating and stunned myocardium. Eur Heart J. 1995:16:Supp. J:19-25.

61. Rahimtoola SH. From coronary artery disease to heart failure: role of hibernating myocardium. Am J Cardiol. 1995:75:16E-22E

62. Jones ER, Childers RF. Contemporary college physics. Don Mills, ON: Addison-Wesley Publishing; 1990:

63. Smith RC, Lange RC. Understanding magnetic resonance imaging. New York: CRC Press, 1998: 1-6.

64. Gadian DG. NMR and its applications to living systems. 2nd edition. Oxford: Oxford University Press, 1995: 1-28.

65. Smith RC, Lange RC. Understanding magnetic resonance imaging. New York: CRC Press, 1998: 29-44.

66. Gadian DG. NMR and its applications to living systems. 2nd edition. Oxford: Oxford University Press, 1995: 139-170.

67. Wood ML, Wehrli FW. Principles of magnetic resonance imaging. In: Stark DD, Bradley WG, eds. Magnetic Resonance Imaging. 3rd edition. St. Louis: Mosby, 1999: 1-14.

68. Schwartz GG, Weiner MW. Magnetic resonance spectroscopy: Basic principles and potential applications in the study of the cardiovascular system. In: Schaefer S, Balaban RS, eds. Cardiovascular magnetic resonance spectroscopy. Dordrecht: Kluwer Academic Publishers, 1993: 1-10.

69. Gadian DG. NMR parameters. 2nd edition. Oxford: Oxford University Press, 1995: 171-205.

70. Camacho SA, Schaefer S. Magnetic resonance spectroscopy of myocardial ischema. In: Schaefer S, Balaban RS, eds. Cardiovascular magnetic resonance spectroscopy. Dordrecht: Kluwer Academic Publishers, 1993: 111-126.

71. Smith RC, Lange RC. Understanding magnetic resonance imaging. New York: CRC Press, 1998: 21-28.

72. Smith RC, Lange RC. Understanding magnetic resonance imaging. New York: CRC Press, 1998: 59-70.

73. Gadian DG. Pulse sequences. In: Gadian DG, ed. NMR and its applications to living systems. 2nd edition. Oxford: Oxford University Press, 1995: 246-277.

74. Smith RC, Lange RC. Understanding magnetic resonance imaging. New York: CRC Press, 1998: 45-58.

75. Nelson KL, Runge VM. Principles of MR contrast. In: Runge VM, ed. Contrast-enhanced clinical magnetic resonance imaging. Kentucky: The University Press of Kentucky. 1995: 1-14.

76. Wolf GL, Halavaara JT. Basic principles of MR contrast agents. Magnetic Resonance Imaging: Clinics of North America. 1996; 4(1): 1-10.

77. Prince MR. Body MR angiography with Gadolinium contrast agents. Magnetic Resonance Imaging: Clinics of North America. 1996; 4(1): 11-24.

78. Nilsson S. MR imaging of contrast-enhanced porcine myocardial infarction: Assessment of reperfusion and tissue viability. Acta Radiol. 1995; 36(suppl. 397: 7-44.

79. Higgins CB. Prediction of myocardial viability by MRI. Circulation. 1999; 99: 727-729

80. Matetzky S, Freimark D, Chouraqui P; Novikov I, Agranat O, Rabinowitz B, Kaplinsky E, Hod H. The distinction between coronary and myocardial reperfusion after thrombolytic therapy by clinical markers of reperfusion. J Am Coll Cardiol. 1998; 32(5): 1326-30.

81. Saeed M, Wendland MF, Masui T, Higging CB. Reperfused myocardial infarctions on T1-and suceptibility-enhanced MRI: Evidence for loss of compartmentalization of contrast media. Magn Reson Med. 1994; 31: 31-39.

82. Kantor HL, Rzedzian RR, Buxton R, Berliner E, Beaulieu P, Rosen B, Brady TJ, Pykett IL. Contrast induced myocardial signal reduction: Effect of lanthanide chelates on ultra high speed MR images. Magn Reson Imaging. 1994; 12: 51-59.

83. Lima JAC, Judd RM, Bazille A, Schulman SP, Atalar E, Zerhouni EA. Regional heterogeneity of human myocardial infarcts demonstrated by contrast-enhanced MRI: Potential Mechanisms. Circulation. 1995; 92: 1117-1125.

84. Ramani K, Judd RM, Holly TA, Parrish TB, Rigolin VH, Parker MA, Callahan C, Fitzgerald SW, Bonow RO, Klocke FJ. Contrast Magnetic Resonance Imaging in the assessment of myocardial viability in patients with stable coronary artery disease and left ventricular dysfunction. Circulation. 1998; 98: 2687-2694.

85. Blackwell GG, Pohost GM. The usefulness of cardiovascular magnetic resonance imaging. Current Problems in Cardiology. 1994; 19(3): 117-176.

86. Balaban RS. Experimental models in cardiac magnetic resonance spectroscopy. In: Schaefer S, Balaban RS, eds. Cardiovascular magnetic resonance spectroscopy. Dordrecht: Kluwer Academic Publishers, 1993: 11-24.

87. Judd RM, Lugo-Olivieri CH, Arai M, Kondo T, Croisille P, Lima JA, Mohan V, Becker LC, Zerhouni EA. Physiological basis of myocardial contrast enhancement in fast magnetic resonance images of 2-day-old reperfused canine infarcts. Circulation. 1995; 92(7): 1902-10.

88. Ito H, Tomooka T, Sokai N, Yu H, Higashino Y, Fujii K, Masuyama T, Kitabatake A, Minamino T. Lack of myocardial perfusion after successful thromolysis. Circulation. 1992; 85: 1699-1705.

89. Lim TH, Lee DH, Kim YH, Park SW, Park PH, Seo DM, Kim ST, Lee TK, Mun CW. Occlusive and reperfused myocardial infarction: detection by using MR imaging with gadolinium polylysine enhancement. Radiology. 1993; 189(3): 756-768.

90. Saeed M, Wendland MF, Yu KK, Lauerma K, Li H-T, Derugin MA, Cavagna FM, Higgins CB. Identification of myocardial reperfusion with echo planar magnetic resonance imaging: Discrimination between occlussive and reperfused infarctions. Circulation. 1994; 90: 1492-1501.

91. Katz IA, Irwig L, Vinen JD, March L, Wyndham LE, Luu T, Nelson GI. Biochemical markers of acute myocardial infarction: strategies for improving their clinical usefulness. Ann Clin Biochem. 1998; 35 (Pt 3): 393-9.

92. Tian G, Shen J, Dai G, Sun J, Xiang B, Luo Z, Somarjai R, Deslauriers R. An interleaved T1-T2* imaging sequence for assessing myocardial injury. J Cardiovasc Magn Reson. 1999; 1: 145-151.

93. Wendland MF, Saeed M, Lauerma K, Derugin N, Mintorovitch J, Cavagna FM, Higgins CB. Alterations in T1 of normal and reperfused infarcted myocardium

after Gd-BOPTA versus GD-DTPA on inversion recovery EPI. Magn Reson Med. 1997; 37: 448-456.

94. Geschwind JFH, Saeed M, Wendland MF, Higgins CB. Depiction of reperfused myocardial infarction using contrast-enhanced spin echo and gradient echo magnetic resonance imaging. Invest Radiol. 1998; 33: 7: 386-392.

95. Geschwind JF, Wendland MF, Saeed M, Lauerma K, Derugin N, Higgins CB. Identification of cell death in reperfused myocardial injury using dual mechanisms of contrast-enhanced magnetic resonance imaging. Acad Radiol. 1994; 1: 319-325.